

COMPARISON OF SHAPE DERIVATIVES USING CUTFEM FOR ILL-POSED BERNOULLI FREE BOUNDARY PROBLEM *

ERIK BURMAN [†], CUIYU HE [‡], AND MATS G. LARSON [§]

Abstract. In this paper we discuss a level set approach for the identification of an unknown boundary in a computational domain. The problem takes the form of a Bernoulli problem where only the Dirichlet datum is known on the boundary that is to be identified, but additional information on the Neumann condition is available on the known part of the boundary. The approach uses a classical constrained optimization problem, where a cost functional is minimized with respect to the unknown boundary, the position of which is defined implicitly by a level set function. To solve the optimization problem a steepest descent algorithm using shape derivatives is applied. In each iteration the cut finite element method is used to obtain high accuracy approximations of the pde-model constraint for a given level set configuration without re-meshing. We consider three different shape derivatives. First the classical one, derived using the continuous optimization problem (optimize then discretize). Then the functional is first discretized using the CutFEM method and the shape derivative is evaluated on the finite element functional (discretize then optimize). Finally we consider a third approach, also using a discretized functional. In this case we do not perturb the domain, but consider a so-called boundary value correction method, where a small correction to the boundary position may be included in the weak boundary condition. Using this correction the shape derivative may be obtained by perturbing a distance parameter in the discrete variational formulation. The theoretical discussion is illustrated with a series of numerical examples showing that all three approaches produce similar result on the proposed Bernoulli problem.

Key words. Ill-posed free boundary Bernoulli problem; Cut Finite Element Method; Level set method; non-fitted mesh;

AMS subject classifications. 65N20,65N21,65N30

1. Introduction. This paper deals with the reconstruction of the free surface of the ill-posed free boundary Bernoulli problem. Comparing to the classical free boundary Bernoulli problem, this paper studies the free boundary problems for which Dirichlet data is known on the free boundary and Cauchy data is known on the fixed boundary. Such problems are found for instance in models where perfectly insulated obstacles [1] need to be detected from data. Following [15] we use the cut finite element method (CutFEM) together with a level set approach in order to numerically identify the free boundary using the shape optimization method. The level set method is a commonly used tool for inverse problems and optimal design [34, 33, 10, 37, 2, 3, 5, 12]. When the level set method is used in the framework of shape optimization or identification, the shape gradient (or steepest descent direction) is obtained by solving partial differential equations in the domain defined by the level set. It is then advantageous to use a fictitious domain type approximation method, provided a sufficient accuracy can be ensured. This is the rationale for combining the CutFEM with level set based optimization. The CutFEM features the following advantages: (1) there is no need to modify the classical basic functions; (2) the

*Submitted to the editors of Journal of Scientific Computing.

Funding: EB and CH were funded by the EPSRC grant EP/P01576X/1. ML was funded by The Swedish Foundation for Strategic Research Grant No. AM13-0029, the Swedish Research Council Grants No. 2017-03911 and the Swedish Research Program Essence

[†]Department of Mathematics, University College London, Gower Street, London, UK-WC1E 6BT, United Kingdom (e.burman@ucl.ac.uk)

[‡]Department of Mathematics, University College London, Gower Street, London, UK-WC1E 6BT, United Kingdom (c.he@ucl.ac.uk)

[§]Department of Mathematics and Mathematical Statistics, Umeå University, SE-90187 Umeå, Sweden (mats.larson@umu.se)

approximation has optimal accuracy in the bulk and on the boundary; and (3) it can easily be used in combination with the *level set method*. It has indeed been applied in combination with the level set approach to various shape or topology optimization problems, for instance in [36, 16, 4, 17].

For the shape optimization method, shape sensitivity analysis plays a paramount role. The objective of the present work is to explore the effect of using different shape derivatives in the shape identification problem described above. First we recall the classical shape derivative obtained by computing the gradient of the Lagrangian functional on the continuous level in an optimize-then-discretize approach. The gradient is then approximated using the cut finite element method. We note here that using the classical optimize-then-discrete approach, the shape derivative has two equivalent forms by the structure theorem of Hadamard-Zolésio [26, 24], i.e., the domain and boundary representations. Assuming enough regularity on the continuous level those two forms are equivalent. The applicability of the domain representation is in principle wider, since it requires lower regularity. Moreover, it has been proven to possess certain super-convergence properties compared to the boundary formulation [29, 28, 30]. In this work, we obtain the domain form for the optimize-then-discretize approach.

One may argue that the discretization of the gradient obtained from the continuous approach only gives an approximate gradient, whose accuracy depends on the mesh-size and that this may prohibit convergence to the minimizer on a fixed mesh. In this paper we therefore aim to derive and study shape derivatives for the CutFEM framework using the discretize-then-optimize approach. The advantage is that the shape derivative obtained by this approach in principle can be exact on the mesh-scale considered. However, since this approach optimizes the discretized system directly, the shape derivative may need more terms for the representation. Another potential problem with this approach is that although the shape derivative is computed using the discrete system, the descent direction in general is not a function in the finite element space and therefore it still needs to be approximated.

Instead of using the complex formula resulting from the discretize-then-optimize approach, it turns out that we can approximate the shape derivative of the discrete formulation in a much more simpler way. The shape derivative of the discrete system may be obtained through the CutFEM method together with a boundary value correction method [9, 19, 31, 22, 20]. Such a boundary value correction type shape derivative, is also exact for the discrete formulation. The derivative only depends on the boundary terms in the Nitsche, or Lagrange multiplier formulation, which could make it possible to tackle more sophisticated problems whose classical shape derivative is difficult to find. The rigorous justification of this boundary value correction shape derivative will be left for future work, instead we will compare its performance numerically with the two other approaches.

To verify and compare the performance of the three different types of derivatives, i.e., the continuous, the discrete and the boundary value correction type, some numerical experiments are presented at the end of this manuscript. Since the objective was to compare the shape derivatives we only consider a simple steepest descent algorithm for the optimization and it is expected that convergence can be enhanced by applying a more sophisticated method such as the Levenberg-Marquard method proposed in [11]. It turns out that all three shape derivatives have similar performance.

For another level set based identification method not relying on shape derivatives we refer to [7, 8].

The paper is organized as follows. In [section 2](#), we introduce the model problem.

Then we introduce the CutFEM for the numerical approximation of the primal and dual solutions in [section 3](#). The various shape derivatives are introduced in [section 4](#). The final optimization algorithm is provided in [section 5](#). Finally, the results for numerical experiments are presented in [section 6](#).

2. Model problem. Let $\hat{\Omega} \subset \mathbb{R}^2$ be a simply connected fixed domain and $\Gamma_f := \partial\hat{\Omega}$. Let \mathcal{O} be a family of bounded connected domains $\Omega \subset \hat{\Omega}$ with the Lipschitz boundary $\partial\Omega = \Gamma_f \cup \Gamma_\Omega$ where Γ_Ω is the free component of the boundary that is to be determined (see [Figure 1](#) for an example). For simplicity, we assume there is no intersection between Γ_Ω and Γ_f . We consider the interior type ill-posed free boundary

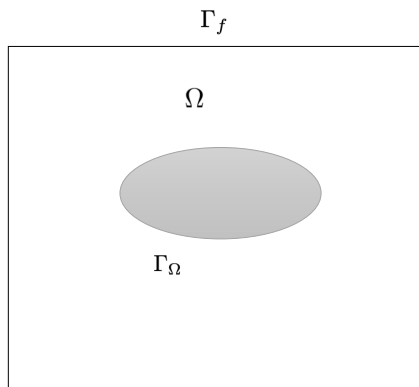


FIG. 1. The domain with the fixed boundary Γ_f and the unknown boundary Γ_Ω

Bernoulli problem, i.e., the fixed boundary Γ_f is exterior to Γ_Ω . Find $\tilde{\Omega} \in \mathcal{O}$ and $u : \tilde{\Omega} \rightarrow \mathbb{R}$ such that

$$(2.1) \quad \begin{aligned} -\Delta u &= f \text{ in } \tilde{\Omega}, \\ u &= 0 \text{ on } \Gamma_{\tilde{\Omega}}, \\ u &= g_D \text{ on } \Gamma_f, \\ D_n u &= g_N \text{ on } \Gamma_f. \end{aligned}$$

Here \mathcal{O} denotes the set of all admissible domains. The datum (f, g_D, g_N) is chosen such that $f \in L^2(\tilde{\Omega})$, $g_D \in H^{1/2}(\Gamma_f)$ and $g_N \in H^{-1/2}(\Gamma_f)$. Here $D_n u = \nabla u \cdot \mathbf{n}$ where \mathbf{n} is the unit outer normal vector to the domain. It is known that, provided the data f, g_D, g_N are compatible with a solution Γ_Ω , this solution is unique. This follows by a unique continuation argument from the Cauchy data on Γ_f . For a proof in the context of scattering problems we refer to [\[23, Theorem 2\]](#).

For an arbitrary $\Omega \in \mathcal{O}$, the system [\(2.1\)](#) is over-determined and therefore the solution may not exist. To represent the interface, we here use the zero level set of a continuous function. The value of level set function away from the interface is not important, provided the gradient of the level set function do not degenerate. To be precise, for each Ω we aim to find a level set function $\phi(\Omega)$ such that

$$(2.2) \quad \phi(x) \begin{cases} > 0 & \text{if } x \notin \Omega, \\ = 0 & \text{if } x \in \Gamma_\Omega, \\ < 0 & \text{if } x \in \Omega. \end{cases}$$

To locate the true free boundary starting from an initial guess Ω , we use a shape optimization procedure that uses a well-posed pair of forward and dual problems. The free boundary is then transported in the optimal direction using an interface transport direction given by the shape derivative of the cost functional.

Define the spaces

$$(2.3) \quad H_{0,\Gamma_\Omega}^1(\Omega) := \{v \in H^1(\Omega) : v = 0 \text{ on } \Gamma_\Omega\}$$

$$(2.4) \quad H_0^1(\Omega) := \{v \in H^1(\Omega) : v = 0 \text{ on } \partial\Omega\}.$$

Let $(\cdot, \cdot)_\Omega$ denote the L^2 -scalar product over $\Omega \subset \mathbb{R}^2$ and $\langle \cdot, \cdot \rangle_\Gamma$ the L^2 -scalar product over the curve $\Gamma \subset \mathbb{R}^2$. The L^2 -norm over a subset X of \mathbb{R}^s , $s = 1, 2$, will be denoted by $\|\cdot\|_X$.

To find an approximation of the solution to the inverse problem (2.1), we solve the following PDE constrained optimization problem: find $\Omega^* \in \mathcal{O}$ such that

$$(2.5) \quad J(\Omega^*) = \min_{\Omega \in \mathcal{O}} J(\Omega) \quad \forall \Omega \in \mathcal{O},$$

where the cost functional is defined by

$$(2.6) \quad J(\Omega) = \frac{1}{2}h^{-1}\|g_D - u(\Omega)\|_{\Gamma_f}^2,$$

where h is the mesh size of the finite element mesh that will be used for the numerical approximation, and $u(\Omega) \in H_{0,\Gamma_\Omega}(\Omega)$ satisfies

$$(2.7) \quad a(u, v) := (\nabla u, \nabla v) = f(v) + \langle g_N, v \rangle_{\Gamma_f} \quad \forall v \in H_{0,\Gamma_\Omega}(\Omega).$$

When there is no risk of ambiguity, we replace $u(\Omega)$ by u .

The corresponding Lagrangian for the constrained minimization problem (2.5) can be formalized as follows:

$$(2.8) \quad \mathcal{L}(\Omega, u(\Omega), v) = \frac{1}{2}h^{-1}\|g_D - u(\Omega)\|_{\Gamma_f}^2 - a(u, v) + l(v)$$

where $l(v) = f(v) + \langle g_N, v \rangle_{\Gamma_f}$.

To find the critical point, denoted by (u, p) , we take the Fréchet derivative with respect to u and v . For the primal variable, u , it yields to solve (2.7). For an arbitrary $\Omega \in \mathcal{O}$, this corresponds to the following forward problem: find $u(\Omega) : \Omega \rightarrow \mathbb{R}$ such that

$$(2.9) \quad \begin{aligned} -\Delta u &= f \text{ in } \Omega, \\ u &= 0 \text{ on } \Gamma_\Omega, \\ D_n u &= g_N \text{ on } \Gamma_f. \end{aligned}$$

For the adjoint solution p , we obtain the weak formulation: find $p \in H_{0,\Gamma_\Omega}^1(\Omega)$ such that

$$(2.10) \quad (\nabla v, \nabla p)_\Omega = h^{-1} \langle u - g_D, v \rangle_{\Gamma_f} \quad \forall v \in H_{0,\Gamma_\Omega}^1(\Omega).$$

Remark 2.1. If $\Omega = \tilde{\Omega}$ we have $u = g_D$ on Γ_f and hence $p \equiv 0$ in $\tilde{\Omega}$.

Remark 2.2. The relation between (2.1) and (2.5) is as follows. If $\tilde{\Omega}$ is the solution to (2.1) and $\tilde{\Omega} \in \mathcal{O}$ then $\tilde{\Omega}$ is the global minimum to (2.5). The converse is also true, by the uniqueness of the inclusion, however there may be local minima that complicate the identification.

3. Approximation of primal and dual solutions using CutFEM. In this section we approximate the primal and dual solution for (2.7) and (2.10), respectively. To solve the primal and dual solutions we use the CutFEM method. The main advantages of using the CutFEM method is that a fixed background mesh of $\hat{\Omega}$ may be used that does not need to fit the moving boundary. The background domain $\hat{\Omega}$ is chosen to be a regular domain, e.g., unit square, such that $\Omega \in \hat{\Omega}$ for all $\Omega \in \mathcal{O}$. Moreover, stability and accuracy of CutFEM, similar to standard FEM is guaranteed given proper stabilization.

Let $\mathcal{T} = \{K\}$ be a shape regular triangular partition of $\hat{\Omega}$ and $h = \max_{K \in \mathcal{T}} h_K$ where h_K is the diameter of K . Define

$$V_h(\Omega) = \{v \in H_1(\Omega) : v|_K \in P_1(K) \forall K \in \mathcal{T}\},$$

and, for $v, w \in V_h(\Omega)$, define

$$(3.1) \quad a_h(w, v) := \tilde{a}_h(w, v) + j(w, v)$$

with

$$(3.2) \quad \tilde{a}_h(w, v) = (\nabla w, \nabla v)_\Omega - \langle D_n w, v \rangle_{\Gamma_\Omega} - \langle D_n v, w \rangle_{\Gamma_\Omega} + \beta h^{-1} \langle w, v \rangle_{\Gamma_\Omega},$$

and

$$(3.3) \quad j(w, v) = \sum_{F \in \mathcal{E}_I} \gamma h \int_F \llbracket D_n w \rrbracket \llbracket D_n v \rrbracket ds,$$

where $\mathcal{E}_I = \{F \subset \partial K : K \in \mathcal{T}; F \cap \partial \hat{\Omega} \neq F\}$ denotes the set of interior faces of the background mesh. The form $j(w, v)$ is the so-called ghost penalty stabilization [13] and $\llbracket \cdot \rrbracket|_F$ denotes the jump operator on F . To simplify the presentation, we here make the ghost penalty stabilization act on all the interior faces. In practice it may be localized to the element faces in the interface zone.

Considering the following variational problems: find $u_h \in V_h(\Omega)$ such that

$$(3.4) \quad a_h(u_h, v) = (f, v)_\Omega + \langle g_N, v \rangle_{\Gamma_f} \quad \forall v \in V_h(\Omega),$$

find $p_h \in V_h(\Omega)$ such that

$$(3.5) \quad a_h(p_h, v) = h^{-1} \langle u_h - g_D, v \rangle_{\Gamma_f} \quad \forall v \in V_h(\Omega).$$

Remark 3.1. Note that in the above formulations all Dirichlet boundary conditions are imposed weakly using Nitsche's method [32].

4. Shape derivatives. In this section, we aim to derive the formulas for different types of shape derivatives. We will first discuss some basic definitions and derive shape derivatives for bulk quantities, this is standard textbook material and essentially follows [35, 24]. Then we extend these arguments to functionals defined on lower dimensional subsets, that are useful for the approximation of the shape derivative of the CutFEM formulation.

4.1. Definition of the shape derivative. For $\Omega \in \mathcal{O}$, we let $W(\Omega, \mathbb{R}^2)$ denote the space of sufficiently smooth vector fields $\boldsymbol{\theta} : \Omega \rightarrow \mathbb{R}^2$ such that $\boldsymbol{\theta} \equiv 0$ on Γ_f . For a vector field $\boldsymbol{\theta} \in W(\Omega, \mathbb{R}^2)$, we define the map

$$(4.1) \quad T_{t, \boldsymbol{\theta}} : x \in \Omega \rightarrow x + t\boldsymbol{\theta}(x) \in \Omega_t(\boldsymbol{\theta}) \subset \mathbb{R}^2.$$

The variable t is interpreted as the pseudo-time. For small t the mapping $\Omega \rightarrow \Omega_t(\boldsymbol{\theta})$ is assumed to be a bijection. We also assume that $\Omega_t(\boldsymbol{\theta}) \in \mathcal{O}$ for any $t \in I = \{-\delta, \delta\}$, with $\delta > 0$ small enough. When there is no risk of confusion, we let $\Omega_t = \Omega_t(\boldsymbol{\theta})$.

The shape derivative of the cost functional $J(\Omega)$ with respect to the domain Ω in the direction of $\boldsymbol{\theta}$ is defined as

$$(4.2) \quad D_{\Omega, \boldsymbol{\theta}} J(\Omega) := \lim_{t \rightarrow 0} \frac{1}{t} (J(\Omega_t(\boldsymbol{\theta})) - J(\Omega)).$$

For a scalar function $v(x, t) : \Omega \times I \rightarrow \mathbb{R}$ that is smooth enough, we define the material derivative in the direction $\boldsymbol{\theta}$ by

$$(4.3) \quad D_{t, \boldsymbol{\theta}} v(x) = \lim_{t \rightarrow 0} \frac{v(x(t), t) - v(x(0), 0)}{t}$$

where $x(t) = T_{t, \boldsymbol{\theta}}(x) = x + t\boldsymbol{\theta}(x)$ and $x(0) = x$. We also define the pseudo-time derivative by

$$(4.4) \quad \partial_t v(x) = \lim_{t \rightarrow 0} \frac{v(x, t) - v(x, 0)}{t}.$$

By the chain rule it is easy to see that

$$(4.5) \quad D_{t, \boldsymbol{\theta}} v = \partial_t v + \boldsymbol{\theta} \cdot \nabla v.$$

The product rule holds for the material derivative:

$$(4.6) \quad D_{t, \boldsymbol{\theta}}(vw) = wD_{t, \boldsymbol{\theta}}v + vD_{t, \boldsymbol{\theta}}w.$$

For future reference, we introduce the notation $\dot{v} := D_{t, \boldsymbol{\theta}}v$ and $v' := \partial_t v$.

LEMMA 4.1. *Let Ω be an open set in \mathbb{R}^2 and $\boldsymbol{\theta} : \mathbb{R}^2 \rightarrow \mathbb{R}^2$ be an injective differentiable mapping. Then the following equalities hold:*

$$(4.7) \quad \begin{aligned} D_{\Omega, \boldsymbol{\theta}} \int_{\Omega} \phi \, dx &= \int_{\Omega} (\dot{\phi} + (\nabla \cdot \boldsymbol{\theta})\phi) \, dx \\ D_{\Omega, \boldsymbol{\theta}} \int_{\Gamma} \psi \, ds &= \int_{\Gamma} (\dot{\psi} + (\nabla_{\Gamma} \cdot \boldsymbol{\theta})\psi) \, ds \end{aligned}$$

where we assume that $\phi(x, t), \psi(x, t) : \mathbb{R}^2 \times I \rightarrow \mathbb{R}$ are functions smooth enough for the expressions of (4.7) to be well defined and where $\nabla_{\Gamma} \cdot \boldsymbol{\theta} = \nabla \cdot \boldsymbol{\theta} - \mathbf{n} \cdot D\boldsymbol{\theta} \cdot \mathbf{n}^t$.

Proof. We give a brief sketch of the proof below to make the presentation self contained. This exposition follows the arguments in [24].

$$\int_{\Omega_t(\boldsymbol{\theta})} \phi(x, t) \, dx = \int_{\Omega} \phi \circ T_{t, \boldsymbol{\theta}} \mu_t \, dx = \int_{\Omega} \phi((x(t), t)) \mu(t) \, dx$$

where $\mu(t) = \det(DT_{t, \boldsymbol{\theta}})$ and $x(t) = x + t\boldsymbol{\theta}(x)$. Note that $\mu(0) = 1$. By definition we have

$$(4.8) \quad \begin{aligned} D_{\Omega, \boldsymbol{\theta}} \int_{\Omega} \phi \, dx &= \lim_{t \rightarrow 0} \frac{1}{t} \left(\int_{\Omega_t(\boldsymbol{\theta})} \phi(x, t) \, dx - \int_{\Omega} \phi(x, 0) \, dx \right) \\ &= \lim_{t \rightarrow 0} \int_{\Omega} \frac{1}{t} (\phi(x(t), t) \mu_t - \phi(x, 0) \mu_0) \, dx \\ &= \int_{\Omega} \dot{\phi}(x, 0) \, dx + \int_{\Omega} \phi(x, 0) \nabla \cdot \boldsymbol{\theta} \, dx \end{aligned}$$

where we have used the fact that (see Example 3.1 in [24])

$$\lim_{t \rightarrow 0} \frac{1}{t} (\mu(t) - \mu(0)) = \nabla \cdot \boldsymbol{\theta}.$$

To prove the second part of (4.7) we have that

$$\int_{\Gamma_{\Omega_t(\boldsymbol{\theta})}} \phi(x, t) dx = \int_{\Gamma_{\Omega}} \phi \circ T_{t, \boldsymbol{\theta}} \omega(t) dx = \int_{\Gamma_{\Omega}} \phi(x(t), t) \omega(t) dx$$

where $\omega(t) = \mu(t) |(DT_{t, \boldsymbol{\theta}})^{-t} \cdot \mathbf{n}|$. Note that $\omega(0) = 1$. Finally, combining the fact that

$$\lim_{t \rightarrow 0} \frac{1}{t} (\omega(t) - \omega(0)) = \nabla \cdot \boldsymbol{\theta} - (D\boldsymbol{\theta} \cdot \mathbf{n}) \cdot \mathbf{n}$$

gives the second part of (4.7). This completes the proof of the lemma. \square

LEMMA 4.2. *The following relation holds:*

$$(4.9) \quad \begin{aligned} D_{\Omega, \boldsymbol{\theta}} \int_{\Omega} \nabla w \cdot \nabla v dx &= \int_{\Omega} (\nabla \cdot \boldsymbol{\theta}) \nabla w \cdot \nabla v - \nabla w \cdot (D\boldsymbol{\theta} + (D\boldsymbol{\theta})^t) \nabla v dx \\ &+ \int_{\Omega} \nabla \dot{w} \cdot \nabla v + \nabla \dot{v} \cdot \nabla w dx, \end{aligned}$$

where we assume that $w(x, t), v(x, t) : \mathbb{R} \times I \rightarrow \mathbb{R}$ are functions smooth enough for (4.9) to be well defined.

Proof. By change of variables, we have

$$(4.10) \quad \begin{aligned} &\lim_{t \rightarrow 0} \frac{1}{t} \left(\int_{\Omega_t(\boldsymbol{\theta})} \nabla w(x, t) \cdot \nabla v(x, t) dx - \int_{\Omega} \nabla w(x, 0) \cdot \nabla v(x, 0) dx \right) \\ &= \lim_{t \rightarrow 0} \frac{1}{t} \left(\int_{\Omega} ((\nabla w \circ T_t) \cdot (\nabla v \circ T_t)) \mu(t) dx - \int_{\Omega} \nabla w(x, 0) \cdot \nabla v(x, 0) dx \right) \\ &= \lim_{t \rightarrow 0} \frac{1}{t} \left(\int_{\Omega} (A(t) \cdot \nabla(w \circ T_t)) \cdot \nabla(v \circ T_t) dx - \int_{\Omega} \nabla w \cdot \nabla v dx \right) \\ &= \int_{\Omega} (A'(t) \cdot \nabla w) \cdot \nabla v + \nabla \dot{w} \cdot \nabla v + \nabla \dot{v} \cdot \nabla w dx, \end{aligned}$$

where we used the chain rule

$$(\nabla u) \circ T_t = DT_{t, \boldsymbol{\theta}}^{-t} \cdot \nabla(u \circ T_t)$$

and introduced $A(t)$ and its derivative

$$(4.11) \quad A(t) = \mu(t) DT_t^{-1} (DT_t)^{-t}, \quad A'(t) = \nabla \cdot \boldsymbol{\theta} I - (D\boldsymbol{\theta} + (D\boldsymbol{\theta})^t),$$

and finally we employed the product rule. This completes the proof of the lemma. \square

4.1.1. Shape derivatives of boundary and face terms. For the sake of simplicity, we denote by $S(\boldsymbol{\theta}) = D\boldsymbol{\theta} + (D\boldsymbol{\theta})^t$.

LEMMA 4.3. *The following relation holds:*

$$(4.12) \quad \begin{aligned} D_{\Omega, \boldsymbol{\theta}} \int_{\Gamma_{\Omega}} (D_n w) v ds &= \int_{\Gamma_{\Omega}} ((\nabla \cdot \boldsymbol{\theta}) (D_n w) v - (S(\boldsymbol{\theta}) \cdot \nabla w) \cdot \mathbf{n} v) ds \\ &+ \int_{\Gamma_{\Omega}} (D_n \dot{w}) v ds + (\nabla w \cdot \mathbf{n}) \dot{v} ds. \end{aligned}$$

where we assume that $w(x, t), v(x, t) : \mathbb{R} \times I \rightarrow \mathbb{R}$ are functions smooth enough for (4.12) to be well defined.

Proof. First by change of variable we have

$$(4.13) \quad \begin{aligned} \int_{\Gamma_{\Omega_t}} \nabla w(x, t) \cdot \mathbf{n}_t v(x, t) ds &= \int_{\Gamma_{\Omega}} (\nabla w \circ T_t) \cdot (\mathbf{n}_t \circ T_t)(v \circ T_t) \omega(t) ds \\ &= \int_{\Gamma_{\Omega}} (DT_t^{-t} \cdot \nabla(w \circ T_t)) \cdot (\mathbf{n}_t \circ T_t)(v \circ T_t) \omega(t) ds. \end{aligned}$$

From Theorem 4.4 in [24] it holds that

$$\mathbf{n}_t \circ T_t = \frac{DT_t^{-t} \cdot \mathbf{n}}{|DT_t^{-t} \cdot \mathbf{n}|}.$$

Recall that $\omega_t = \mu(t)|DT_t^{-t} \cdot \mathbf{n}|$. By a direct calculation we have

$$(4.14) \quad \int_{\Gamma_{\Omega_t}} (\nabla w(x, t) \cdot \mathbf{n}_t) v(x, t) ds = \int_{\Gamma_{\Omega}} (A(t) \cdot \nabla(w \circ T_t)) \cdot \mathbf{n}(v \circ T_t) ds$$

Finally, combing (4.14) and (4.11) gives

$$(4.15) \quad \begin{aligned} D_{\Omega, \boldsymbol{\theta}} \int_{\Gamma_{\Omega}} \nabla w \cdot \mathbf{n} v ds &= \int_{\Gamma_{\Omega}} (A'(t) \cdot (\nabla w \cdot \mathbf{n})v + (\nabla \dot{w} \cdot \mathbf{n})v) ds + (\nabla w \cdot \mathbf{n}) \dot{v} ds \\ &= \int_{\Gamma_{\Omega}} ((\nabla \cdot \boldsymbol{\theta})(\nabla w \cdot \mathbf{n})v - (S(\boldsymbol{\theta}) \cdot \nabla w) \cdot \mathbf{n}v + (\nabla w \cdot \mathbf{n}) \dot{v} ds + (\nabla \dot{w} \cdot \mathbf{n})v) ds. \end{aligned}$$

This completes the proof of the lemma. \square

The stability of the CutFEM method is ensured by the ghost penalty term. In the following Lemma we give a result allowing the integration of the effect of this term in the shape gradient. The proof is given in the appendix.

LEMMA 4.4. *Assume that $w, v \in H^1(\Omega, t)$ and that locally on each triangle K , $w(x, t)|_K, v(x, t)|_K \in H^{3/2+\epsilon}(K)$. Then there holds*

$$(4.16) \quad D_{\Omega, \boldsymbol{\theta}} \int_F \llbracket D_n w \rrbracket \llbracket D_n v \rrbracket ds = \int_F (\llbracket \nabla \dot{w} \cdot \mathbf{n} \rrbracket \llbracket \nabla v \cdot \mathbf{n} \rrbracket + \llbracket \nabla w \cdot \mathbf{n} \rrbracket \llbracket \nabla \dot{v} \cdot \mathbf{n} \rrbracket) ds + \epsilon_F(w, v)$$

where

$$(4.17) \quad \begin{aligned} \epsilon_F(w, v) &= \int_F \llbracket (\nabla \cdot \boldsymbol{\theta}) \nabla w \cdot \mathbf{n} - \nabla w \cdot S(\boldsymbol{\theta}) \cdot \mathbf{n} \rrbracket \llbracket \nabla v \cdot \mathbf{n} \rrbracket ds \\ &\quad + \int_F \llbracket (\nabla \cdot \boldsymbol{\theta}) \nabla v \cdot \mathbf{n} - \nabla v \cdot S(\boldsymbol{\theta}) \cdot \mathbf{n} \rrbracket \llbracket \nabla w \cdot \mathbf{n} \rrbracket ds \\ &\quad - \int_F \llbracket \nabla w \cdot \mathbf{n} \rrbracket \llbracket \nabla v \cdot \mathbf{n} \rrbracket (\nabla \cdot \boldsymbol{\theta} - (D\boldsymbol{\theta} \cdot \mathbf{n}) \cdot \mathbf{n}) ds. \end{aligned}$$

4.2. Optimize-then-discretize approach. In this subsection we first analyse the shape optimization based on the optimize-then-discretize approach, i.e., the representation for the shape derivative is computed based on the continuous problems.

In the numerical approximation, we will simply replace the continuous solutions by the numerical ones. Note that for this approach the formula of the shape derivative is then independent of the numerical method used to approximate the solutions. Therefore, the shape derivative is not exact since by assumption its input is assumed to be the true solutions while in reality it is evaluated using their approximations. The error in the gradient will be of optimal order asymptotically, if the CutFEM solution has optimal error estimates in $W^{1,4}(\Omega)$ and $L^4(\Omega)$, see [15].

On $\Omega_t(\boldsymbol{\theta})$, $t \in [0, \tau]$ we define $u(x, t) \in H_{0,\Gamma\Omega_t}^1$ and $p(x, t) \in H_{0,\Gamma\Omega_t}^1$ such that

$$(4.18) \quad (\nabla u(x, t), \nabla v)_{\Omega_t} = (f, v)_{\Omega_t} + \langle g_N, v \rangle_{\Gamma_f} \quad \forall v \in H_{0,\Gamma\Omega_t}^1$$

and

$$(4.19) \quad (\nabla v, \nabla p(x, t))_{\Omega_t} = h^{-1} \langle u(x, t) - g_D, v \rangle_{\Gamma_f} \quad \forall v \in H_{0,\Gamma\Omega_t}^1.$$

Immediately we have that $\dot{p} = \dot{u} = 0$ on Γ_Ω , therefore $\dot{u} \in H_{0,\Gamma\Omega}(\Omega)$ and $\dot{p} \in H_{0,\Gamma\Omega}(\Omega)$.

LEMMA 4.5. *Let \mathcal{L} be defined in (2.8). Then its shape derivative has the following representation:*

$$(4.20) \quad \begin{aligned} & D_{\Omega,\boldsymbol{\theta}}\mathcal{L}(\Omega, u(\Omega), p(\Omega)) \\ &= \int_{\Omega} (\nabla \cdot \boldsymbol{\theta}) (fp - \nabla u \cdot \nabla p) \, dx + \int_{\Omega} \nabla u \cdot S(\boldsymbol{\theta}) \cdot \nabla p \, dx + \int_{\Omega} (\nabla f \cdot \boldsymbol{\theta}) p \, dx. \end{aligned}$$

Proof. Rearrange $\mathcal{L}(\Omega, u, p)$ such that

$$(4.21) \quad \mathcal{L}(\Omega, u, p) \triangleq \mathcal{A}_1 + \mathcal{A}_2$$

where

$$\mathcal{A}_1 = -(\nabla u, \nabla p)_{\Omega} + (f, p)_{\Omega}, \quad \mathcal{A}_2 = \frac{1}{2} h^{-1} \langle g_D - u, g_D - u \rangle_{\Gamma_f} + \langle g_N, p \rangle_{\Gamma_f}.$$

By Lemma 4.1 and Lemma 4.2, we firstly have

$$(4.22) \quad \begin{aligned} D_{\boldsymbol{\theta},\Omega}\mathcal{A}_1 &= -(\nabla \cdot \boldsymbol{\theta}, \nabla u \cdot \nabla p - fp)_{\Omega} + \int_{\Omega} \nabla u \cdot S(\boldsymbol{\theta}) \cdot \nabla p \, dx \\ &\quad - (\nabla \dot{u}, \nabla p)_{\Omega} - (\nabla u, \nabla \dot{p})_{\Omega} + (\dot{f}, p)_{\Omega} + (f, \dot{p})_{\Omega}. \end{aligned}$$

Note that $\dot{f} = \nabla f \cdot \boldsymbol{\theta}$ since $f' = 0$. Thanks to the fact that $\dot{u} \in H_{0,\Gamma\Omega}(\Omega)$ and $\dot{p} \in H_{0,\Gamma\Omega}(\Omega)$, by (2.7) and (2.10) we have

$$(4.23) \quad \begin{aligned} -(\nabla \dot{u}, \nabla p)_{\Omega} - (\nabla u, \nabla \dot{p})_{\Omega} + (f, \dot{p})_{\Omega} &= -h^{-1} \langle u - g_D, \dot{u} \rangle_{\Gamma_f} - \langle g_N, \dot{p} \rangle_{\Gamma_f} \\ &= -h^{-1} \langle u - g_D, u' \rangle_{\Gamma_f} - \langle g_N, p' \rangle_{\Gamma_f}. \end{aligned}$$

Note that on Γ_f , we have used the fact that $\dot{u} = u'$ and $\dot{p} = p'$, since $\boldsymbol{\theta} = 0$ on Γ_f . By the product and chain rule we immediately have

$$(4.24) \quad D_{\boldsymbol{\theta},\Omega}\mathcal{A}_2 = h^{-1} \langle u - g_D, u' \rangle_{\Gamma_f} + \langle g_N, p' \rangle_{\Gamma_f}.$$

Combining the identities gives (4.20). This completes the proof of the lemma. \square

4.3. Discretize-then-optimize approach. In this subsection we aim to derive the shape derivative formula for the approach where we first discretize the Lagrangian using the CutFEM method and then we evaluate the shape derivative of the discrete functional. For this case the optimization analysis is dependent on the numerical solutions and the numerical method that is used. As a consequence the shape derivative is exact for the discrete functional.

Starting from the Lagrangian (2.8) we obtain the discrete Lagrangian form by replacing the bilinear and linear forms a and l by the corresponding discrete forms a_h (defined in (3.1)) and $l_h(v)$:

$$(4.25) \quad \mathcal{L}_h(\Omega, w_h, v_h) = \frac{1}{2}h^{-1}\|g_D - w_h\|_{\Gamma_f}^2 - a_h(w_h, v_h) + l_h(v_h).$$

Note that taking the Fréchet derivative with respect to v_h and w_h in (4.25) gives exactly the CutFEM formulation for u_h and p_h in (3.4) and (3.5), respectively.

To define the shape derivative, firstly we need to define the function space for $u_h(x, t)$ and $p_h(x, t)$ on Ω_t . We do this by using a pullback map to Ω where the elements are triangular and use the standard definition of the finite element space on the reference domain.

For each $K \in \mathcal{T}_h$, let $K^t = T_{t,\theta}K$. When there is no risk of ambiguity, we replace $T_{t,\theta}$ by T_t . Here we assume that $T_t \in [C^1(\Omega)]^d$. Then, by the inverse function theorem, T_t is a bijection for sufficiently small t and its derivatives are point wise well defined. We also define $\mathcal{T}_h^t := \{K^t, K \in \mathcal{T}_h\}$ and

$$V_h^t(\Omega_t) := \{v \in H^1(\mathcal{T}_h^t), v|_{K^t} \in V_h^t(K^t)\}$$

where $V_h^t(K^t)$ satisfies $V_h^t(K^t) = V_h(K) \circ T_t^{-1}$. It is then easy to verify that

$$v_h^t \circ T_t \in V_h(\Omega) \quad \forall v_h^t \in V_h^t(\Omega_t).$$

We now define $u_h(x, t)$ and $p_h(x, t)$ on Ω_t . Let $u_h(x, t)$ and $p_h(x, t)$ be the solution of (3.4) and (3.5) in the mapped space $V_h^t(\Omega_t)$ using integrals over Ω_t and Γ_{Ω_t} , respectively instead of Ω and Γ_Ω .

LEMMA 4.6. *Let $u_h(x, t)$ and $p_h(x, t)$ be defined as above. Then*

$$(4.26) \quad \dot{u}_h \in V_h(\Omega) \quad \text{and} \quad \dot{p}_h \in V_h(\Omega).$$

Proof. By the definition, we have that

$$(4.27) \quad \begin{aligned} \dot{u}_h(x) &= \lim_{t \rightarrow 0} \frac{1}{t} (u_h(x(t), t) - u_h(x, 0)) \\ &= \lim_{t \rightarrow 0} \frac{1}{t} (u_h(T_t(x), t) - u_h(x, 0)). \end{aligned}$$

Since both $u_h(T_t(x), t) \in V_h$ and $u_h(x, 0) \in V_h$, we have that $\dot{u}_h \in V_h$. The result for \dot{p}_h holds by the same argument. \square

In the following lemma we derive the integral representation for the shape derivative of \mathcal{L}_h .

LEMMA 4.7. *Let \mathcal{L}_h be defined in (4.25). Then its shape derivative has the following representation:*

$$\begin{aligned}
 & D_{\Omega, \boldsymbol{\theta}} \mathcal{L}_h(\Omega, u_h(\Omega), p_h(\Omega)) \\
 &= \int_{\Omega} (\nabla \cdot \boldsymbol{\theta}) (f p_h - \nabla u_h \cdot \nabla p_h) dx \\
 &+ \int_{\Omega} (\nabla u_h) S(\boldsymbol{\theta}) (\nabla p_h)^t dx + \int_{\Omega} (\nabla f \cdot \boldsymbol{\theta}) p_h dx \\
 (4.28) \quad &+ \int_{\Gamma_{\Omega}} (\nabla \cdot \boldsymbol{\theta}) (D_n u_h) p_h - (S(\boldsymbol{\theta}) \cdot \nabla u_h) \cdot \mathbf{n} p_h ds \\
 &+ \int_{\Gamma_{\Omega}} (\nabla \cdot \boldsymbol{\theta}) (D_n p_h) u_h - (S(\boldsymbol{\theta}) \cdot \nabla p_h) \cdot \mathbf{n} u_h ds \\
 &- \int_{\Gamma_{\Omega}} \beta h^{-1} (\nabla_{\Gamma} \cdot \boldsymbol{\theta}) u_h p_h + \sum_{F \in \mathcal{E}_I} \gamma h \epsilon_F(u_h, p_h)
 \end{aligned}$$

Proof. Rearrange $\mathcal{L}(\Omega, u, p)$ such that

$$(4.29) \quad \mathcal{L}(\Omega, u, p) \triangleq \sum_{i=1}^4 \mathcal{A}_i$$

where

$$\begin{aligned}
 \mathcal{A}_1 &= -(\nabla u_h, \nabla p_h)_{\Omega} + (f, p_h)_{\Omega}, \\
 \mathcal{A}_2 &= \frac{1}{2} h^{-1} \langle g_D - u_h, g_D - u_h \rangle_{\Gamma_f} + \langle g_N, p_h \rangle_{\Gamma_f}, \\
 \mathcal{A}_3 &= \langle D_n u_h, p_h \rangle_{\Gamma_{\Omega}} + \langle D_n p_h, u_h \rangle_{\Gamma_{\Omega}} - \beta h^{-1} \langle u_h, p_h \rangle_{\Gamma_{\Omega}}, \\
 \mathcal{A}_4 &= -j(u_h, p_h).
 \end{aligned}$$

For the first two terms, we could derive its shape derivative similarly as in Lemma 4.5:

$$\begin{aligned}
 (4.30) \quad D_{\boldsymbol{\theta}, \Omega} \mathcal{A}_1 &= - \int_{\Omega} (\nabla \cdot \boldsymbol{\theta}) (\nabla u_h \cdot \nabla p_h - f p_h) ds + \int_{\Omega} (\nabla u_h) S(\boldsymbol{\theta}) (\nabla p_h)^t dx + \int_{\Omega} (\nabla f \cdot \boldsymbol{\theta}) p_h dx \\
 &- \int_{\Omega} (\nabla \dot{u}_h \cdot \nabla p_h) dx - \int_{\Omega} (\nabla u_h \cdot \nabla \dot{p}_h) dx + \int_{\Omega} (f \dot{p}_h) dx. \quad \blacksquare
 \end{aligned}$$

Similarly, we have

$$(4.31) \quad D_{\boldsymbol{\theta}, \Omega} \mathcal{A}_2 = -h^{-1} \langle g_D - u_h, \dot{u}_h \rangle_{\Gamma_f} + \langle g_N, \dot{p}_h \rangle_{\Gamma_f}.$$

For \mathcal{A}_3 , by Lemma 4.3 we have

$$\begin{aligned}
 (4.32) \quad D_{\boldsymbol{\theta}, \Omega} \mathcal{A}_3 &= \int_{\Gamma_{\Omega}} (\nabla \cdot \boldsymbol{\theta}) (D_n u_h) p_h - (S(\boldsymbol{\theta}) \cdot \nabla u_h) \cdot \mathbf{n} p_h + (D_n \dot{u}_h) p_h + (D_n u_h) \dot{p}_h ds \\
 &+ \int_{\Gamma_{\Omega}} ((\nabla \cdot \boldsymbol{\theta}) (D_n p_h) u_h - (S(\boldsymbol{\theta}) \cdot \nabla p_h) \cdot \mathbf{n} u_h + (D_n \dot{p}_h) u_h + (D_n p_h) \dot{u}_h) ds \\
 &- \beta h^{-1} \int_{\Gamma_{\Omega}} (\nabla_{\Gamma} \cdot \boldsymbol{\theta}) u_h p_h + \dot{u}_h p_h + u_h \dot{p}_h ds.
 \end{aligned}$$

And for \mathcal{A}_4 by [Lemma 4.4](#) we have

$$(4.33) \quad D_{\boldsymbol{\theta}, \Omega} \mathcal{A}_4 = -j(u_h, \dot{p}_h) - j(\dot{u}_h, p_h) - \sum_{F \in \mathcal{E}_I} \gamma \epsilon_F(u_h, p_h).$$

Thanks to the fact that $\dot{u}_h \in V_h$ and $\dot{p}_h \in V_h$, by [\(3.4\)](#) and [\(3.5\)](#) with v replaced by \dot{p}_h in [\(3.4\)](#) and by \dot{u}_h in [\(3.5\)](#) we have

$$(4.34) \quad \begin{aligned} 0 &= -(\nabla \dot{u}_h, \nabla p_h)_\Omega - (\nabla u_h, \nabla \dot{p}_h)_\Omega + (f, \dot{p}_h)_\Omega \\ &\quad - h^{-1} \langle g_D - u_h, \dot{u}_h \rangle_{\Gamma_f} + \langle g_N, \dot{p}_h \rangle_{\Gamma_f} \\ &\quad + \langle D_n \dot{u}_h, p_h \rangle_{\Gamma_\Omega} + \langle D_n u_h, \dot{p}_h \rangle_{\Gamma_\Omega} + \langle D_n \dot{p}_h, u_h \rangle_{\Gamma_\Omega} + \langle D_n p_h, \dot{u}_h \rangle_{\Gamma_\Omega} \quad \square \\ &\quad - \beta h^{-1} \langle \dot{u}_h, p_h \rangle_{\Gamma_\Omega} - \beta h^{-1} \langle u_h, \dot{p}_h \rangle_{\Gamma_\Omega} \\ &\quad - j(u_h, \dot{p}_h) - j(\dot{u}_h, p_h). \end{aligned}$$

Combing [\(4.29\)](#)–[\(4.34\)](#) gives [\(4.28\)](#).

Remark 4.8. The shape derivative is exact, however, due to the extra terms of the CutFEM formulation it becomes more complicated. We also observe that the field $\boldsymbol{\theta}$ still has to be approximated in the finite element space (see [section 5.1](#) below).

4.4. CutFEM using boundary value correction. In the classical shape derivative the function $u(x, t)$ and $p(x, t)$ are defined on the domain of Ω_t . In this subsection, we instead define $u(x, t)$ on Ω (instead of Ω_t) for t small enough and include the effect of perturbations of the domain on the boundary through the weakly imposed boundary conditions, i.e., the boundary correction approach. The idea of perturbing boundary conditions to improve geometry approximation was first introduced in [\[9\]](#). The extension to CutFEM was considered in [\[19\]](#). For a recent discussion of the method interpreted as a singular Robin condition we refer to [\[25\]](#). Similar ideas have already been exploited in the context of the standard Bernoulli problem, see [\[6\]](#). Drawing on the ideas on boundary correction for the CutFEM method [\[19\]](#) we modify the weak formulation on the free boundary as follows:

$$(4.35) \quad \tilde{a}_h^t(w, v) = (\nabla w, \nabla v)_\Omega - \langle D_n w, v \rangle_{\Gamma_\Omega} - \langle D_n v, w \circ T_t \rangle_{\Gamma_\Omega} + \beta h^{-1} (w \circ T_t, v \circ T_t)_{\Gamma_\Omega},$$

and

$$a_h^t(v, w) := \tilde{a}_h^t(v, w) + j(v, w).$$

We note that the above weak formulation is consistent with the following:

$$-\Delta u = f \in \Omega, \quad D_n u = g_N \text{ on } \Gamma_f, \quad \text{and} \quad u = 0 \text{ on } \Gamma_{\Omega_t}.$$

Also note that the Dirichlet boundary condition that is originally weakly imposed on Γ_Ω is now weakly imposed on Γ_{Ω_t} through function composition.

Now, considering the following variational problems: finding $u_h(x, t) \in V_h(\Omega)$ such that

$$(4.36) \quad a_h^t(u_h(x, t), v) = (f, v)_\Omega + \langle g_N, v \rangle_{\Gamma_f} \quad \forall v \in V_h(\Omega),$$

and finding $p_h(x, t) \in V_h(\Omega)$ such that

$$(4.37) \quad a_h^t(v, p_h(x, t)) = h^{-1} \langle u_h(t) - g_D, v \rangle_{\Gamma_f} \quad \forall v \in V_h(\Omega).$$

We define the corresponding Lagrangian at pseudo-time t with respect to $\boldsymbol{\theta}$,

$$(4.38) \quad \begin{aligned} \mathcal{L}_h^t(\Omega, u_h(t), p_h(t)) &= \frac{1}{2} h^{-1} \|g_D - u_h(x, t)\|_{\Gamma_f}^2 - a_h^t(u_h(x, t), p_h(x, t)) \\ &\quad + (f, p_h(x, t))_\Omega + \langle g_N, p_h(x, t) \rangle_{\Gamma_f}. \end{aligned}$$

Remark 4.9. It is easy to see that

$$\lim_{t \rightarrow 0} \mathcal{L}_h^t(\Omega, u_h(t), p_h(t)) = \mathcal{L}_h(\Omega, u_h, p_h).$$

Finally, for a given $\boldsymbol{\theta}$, we define the modified shape derivative by

$$(4.39) \quad \tilde{D}_{\Omega, \boldsymbol{\theta}} \mathcal{L}_h = \lim_{t \rightarrow 0} \frac{1}{t} (\mathcal{L}_h^t(\Omega, u_h(t), p_h(t)) - \mathcal{L}_h(\Omega, u_h(0), p_h(0))),$$

where $u_h(0) = u_h(\Omega)$, $p_h = p_h(\Omega)$ are the solutions on Ω for (3.4) and (3.5), respectively.

Remark 4.10. We note that contrary to the classical shape derivative here $u_h(x, t)$ and $p_h(x, t)$ are still defined on the fixed Ω and not on the perturbed domain $\Omega_t = \Omega + t\boldsymbol{\theta}$.

4.5. Shape derivative formula based on the boundary value correction.

In this subsection we derive the explicit formula of (4.39) in terms of $u_h(\Omega)$ and $p_h(\Omega)$.

Recall the pseudo-time derivative for u_h and p_h :

$$(4.40) \quad u'_h(x) = \lim_{t \rightarrow 0} \frac{1}{t} (u_h(x, t) - u_h(x, 0)), \quad q'_h(x) = \lim_{t \rightarrow 0} \frac{1}{t} (q_h(x, t) - q_h(x, 0)) \quad \forall x \in \Omega.$$

LEMMA 4.11. *Let u_h and p_h be the solutions of (3.4) and (3.5), respectively. We have the following expression for the modified shape derivative defined in (4.39):*

$$(4.41) \quad \tilde{D}_{\Omega, \boldsymbol{\theta}} \mathcal{L}_h = \langle D_n p_h, \nabla u_h \cdot \boldsymbol{\theta} \rangle_{\Gamma_\Omega} - \beta h^{-1} (\langle \nabla u_h \cdot \boldsymbol{\theta}, p_h \rangle_{\Gamma_\Omega} + \langle u_h, \nabla p_h \cdot \boldsymbol{\theta} \rangle_{\Gamma_\Omega}).$$

Proof. By definition we have

$$(4.42) \quad \begin{aligned} \tilde{D}_{\Omega, \boldsymbol{\theta}} \mathcal{L}_h &= \lim_{t \rightarrow 0} \frac{1}{t} (\mathcal{L}_h^t(\Omega, u_h(t), p_h(t)) - \mathcal{L}_h(\Omega, u_h(0), p_h(0))) \\ &= \lim_{t \rightarrow 0} \frac{1}{2t} h^{-1} \langle u_h(t) - g_D \rangle_{\Gamma_f}^2 - \langle u_h(0) - g_D \rangle_{\Gamma_f}^2 \\ &\quad - \lim_{t \rightarrow 0} \frac{1}{t} (a_h^t(u_h(t), p_h(t)) - a_h(u_h(0), p_h(0))) \\ &\quad + \lim_{t \rightarrow 0} \frac{1}{t} (f, p_h(t) - p_h(0))_\Omega + \lim_{t \rightarrow 0} \frac{1}{t} \langle g_N, p_h(t) - p_h(0) \rangle_{\Gamma_f} \\ &\quad - \lim_{t \rightarrow 0} \frac{1}{t} (j(u_h(t), p_h(t)) - j(u_h(0), p_h(0))) \\ &\triangleq \sum_{i=1}^5 \mathcal{A}_i. \end{aligned}$$

By a direct calculation and (4.40) we have

$$(4.43) \quad \mathcal{A}_1 = h^{-1} \langle u_h - g_D, u'_h \rangle_{\Gamma_f}, \quad \mathcal{A}_3 = (f, p'_h)_\Omega,$$

$$(4.44) \quad \mathcal{A}_4 = \langle g_N, p'_h \rangle_{\Gamma_f}, \quad \mathcal{A}_5 = -(j(u'_h, p_h) - j(u_h, p'_h)).$$

Expanding and regrouping terms in $a_h^t(\cdot)$ and $a_h(\cdot)$ gives

$$\begin{aligned}
(4.45) \quad -\mathcal{A}_2 &= \lim_{t \rightarrow 0} \frac{1}{t} (a_h^t(u_h(t), p_h(t)) - a_h(u_h, p_h)) \\
&= \lim_{t \rightarrow 0} \frac{1}{t} ((\nabla u_h(t), \nabla p_h(t))_\Omega - (\nabla u_h(0), \nabla p_h(0))_\Omega) \\
&\quad - \lim_{t \rightarrow 0} \frac{1}{t} (\langle D_n u_h(t), p_h(t) \rangle_{\Gamma_\Omega} - \langle D_n u_h(0), p_h(0) \rangle_{\Gamma_\Omega}) \\
&\quad - \lim_{t \rightarrow 0} \frac{1}{t} (\langle D_n p_h(t), u_h(t) \circ T_t \rangle_{\Gamma_\Omega} - \langle D_n p_h(0), u_h(0) \rangle_{\Gamma_\Omega}) \\
&\quad + \lim_{t \rightarrow 0} \frac{1}{t} \beta h^{-1} (\langle u_h(t) \circ T_t, p_h(t) \circ T_t \rangle_{\Gamma_\Omega} - \langle u_h(0), p_h(0) \rangle_{\Gamma_\Omega}).
\end{aligned}$$

Applying the product rule, Taylor expansion and neglecting the higher order terms gives

$$\begin{aligned}
(4.46) \quad -\mathcal{A}_2 &= \lim_{t \rightarrow 0} \frac{1}{t} (a_h^t(u_h(t), p_h(t)) - a_h(u_h, p_h)) \\
&= ((\nabla u_h', p_h)_\Omega + (\nabla u_h, \nabla p_h')_\Omega) - (\langle D_n u_h', p_h \rangle_{\Gamma_\Omega} - \langle D_n u_h, p_h' \rangle_{\Gamma_\Omega}) \\
&\quad - \lim_{t \rightarrow 0} \frac{1}{t} (\langle D_n p_h(t), u_h(t) + t \nabla u_h(t) \cdot \boldsymbol{\theta} \rangle_{\Gamma_\Omega} - \langle D_n p_h, u_h \rangle_{\Gamma_\Omega}) \\
&\quad + \lim_{t \rightarrow 0} \frac{1}{t} \beta h^{-1} (\langle u_h(t) + t \nabla u_h(t) \cdot \boldsymbol{\theta}, p_h(t) + t \nabla p_h(t) \cdot \boldsymbol{\theta} \rangle_{\Gamma_\Omega} - \langle u_h, p_h \rangle_{\Gamma_\Omega}) \\
&= ((\nabla u_h', \nabla p_h)_\Omega + (\nabla u_h, \nabla p_h')_\Omega) - (\langle D_n u_h', p_h \rangle_{\Gamma_\Omega} - \langle D_n u_h, p_h' \rangle_{\Gamma_\Omega}) \\
&\quad - (\langle D_n p_h', u_h \rangle_{\Gamma_\Omega} + \langle D_n p_h, u_h' \rangle_{\Gamma_\Omega} + \langle D_n p_h, \nabla u_h \cdot \boldsymbol{\theta} \rangle_{\Gamma_\Omega}) \\
&\quad + \beta h^{-1} (\langle u_h', p_h \rangle_{\Gamma_\Omega} + \langle u_h, p_h' \rangle_{\Gamma_\Omega} + \langle \nabla u_h \cdot \boldsymbol{\theta}, p_h \rangle_{\Gamma_\Omega} + \langle u_h, \nabla p_h \cdot \boldsymbol{\theta} \rangle_{\Gamma_\Omega}).
\end{aligned}$$

Note that $u_h', p_h' \in V_h$. By (3.4) and (3.5) we have

$$\begin{aligned}
(4.47) \quad &a_h(p_h, u_h') \\
&= (\nabla p_h, \nabla u_h')_\Omega - \langle D_n p_h, u_h' \rangle_{\Gamma_\Omega} - \langle D_n u_h', p_h \rangle_{\Gamma_\Omega} + \beta h^{-1} \langle p_h, u_h' \rangle_{\Gamma_\Omega} + j(p_h, u_h') \\
&= h^{-1} \langle u_h - g_D, u_h' \rangle_{\Gamma_f}
\end{aligned}$$

and

$$\begin{aligned}
(4.48) \quad &a_h(u_h, p_h') \\
&= (\nabla u_h, \nabla p_h')_\Omega - \langle D_n u_h, p_h' \rangle_{\Gamma_\Omega} - \langle D_n p_h', u_h \rangle_{\Gamma_\Omega} + \beta h^{-1} \langle u_h, p_h' \rangle_{\Gamma_\Omega} + j(u_h, p_h') \\
&= (f, u_h')_\Omega + \langle g_N, p_h' \rangle_{\Gamma_f}
\end{aligned}$$

Combining (4.42)–(4.48) gives (4.41). This completes the proof of the lemma. \square

Remark 4.1. Applying the Taylor expansion and omitting the higher order terms gives

$$\begin{aligned}
(4.49) \quad a_h^t(w, v) &\approx (\nabla w, \nabla v)_\Omega - \langle D_n w, v \rangle_{\Gamma_\Omega} - \langle D_n v, w \rangle_{\Gamma_\Omega} + \beta h^{-1} \langle w, v \rangle_{\Gamma_\Omega} \\
&\quad - t (\langle D_n v, \nabla w \cdot \boldsymbol{\theta} \rangle_{\Gamma_\Omega} + \beta h^{-1} \langle \nabla w \cdot \boldsymbol{\theta}, v \rangle_{\Gamma_\Omega} + \beta h^{-1} \langle \nabla v \cdot \boldsymbol{\theta}, w \rangle_{\Gamma_\Omega}).
\end{aligned}$$

Taking the derivative with respect to t also gives (4.41).

Remark 4.2. We note that here the modified shape derivative $\tilde{D}_{\Omega, \boldsymbol{\theta}}$ is exact. However, comparing to (4.28) the formula in (4.41) is much more simple. Furthermore, since the shape derivative has the surface form and it is exact, it would be an interesting alternative when an explicit parametric approach for the surface representation is used.

5. Optimization algorithms. The objective is now to find the vector field $\boldsymbol{\theta} : \hat{\Omega} \rightarrow \hat{\Omega}$ such that $J(\Omega)$ decreases the fastest along that direction. We seek through solving the following constrained minimization problem: starting from the domain Ω with free boundary Γ_Ω we wish to find the steepest descent vector field $\boldsymbol{\beta} \in W(\hat{\Omega}, \mathbb{R}^d)$ such that

$$(5.1) \quad \boldsymbol{\beta} = \underset{\substack{\|\boldsymbol{\theta}\|_{H^1(\hat{\Omega})}=1, \\ \boldsymbol{\theta}=0 \text{ on } \Gamma_f.}}{\operatorname{argmin}} D_{\Omega, \boldsymbol{\theta}} \mathcal{L}_h.$$

Define the corresponding Lagrangian

$$\mathcal{K}(\boldsymbol{\theta}, \lambda) = D_{\Omega, \boldsymbol{\theta}} \mathcal{L}_h + \lambda (\|\boldsymbol{\theta}\|_{H^1(\hat{\Omega})}^2 - 1),$$

and taking the derivative with respect to λ gives the constrain condition. From remark 4.1 in [15], an equivalent formulation of (5.1) renders to find $\tilde{\boldsymbol{\beta}} \in H_0^1(\hat{\Omega})^d$ such that

$$(5.2) \quad (\tilde{\boldsymbol{\beta}}, \boldsymbol{\theta})_{H^1(\hat{\Omega})} = -D_{\Omega, \boldsymbol{\theta}} \mathcal{L}_h \quad \forall \boldsymbol{\theta} \in H_0^1(\hat{\Omega})^d.$$

where $\tilde{\boldsymbol{\beta}} = 2\lambda\boldsymbol{\beta}$ and $\lambda = \frac{\|\tilde{\boldsymbol{\beta}}\|_{H^1(\hat{\Omega})}}{2}$. Then it is easy to see that by taking $\boldsymbol{\theta} = \boldsymbol{\beta}$

$$D_{\Omega, \boldsymbol{\beta}} \mathcal{L}_h = -(\tilde{\boldsymbol{\beta}}, \boldsymbol{\beta})_{H^1(\hat{\Omega})} = -\|\tilde{\boldsymbol{\beta}}\|_{H_0^1(\hat{\Omega})} < 0$$

which guarantees that $\boldsymbol{\beta}$ is a descent direction.

The following Hadamard Lemma indicates that under certain regularity the variational problem (5.2) is equivalent to an interface problem.

Lemma 5.1 (Hadamard). If $\mathcal{L}(\cdot)$ is shape differentiable at every element Ω of class C^k , $\Omega \subset \hat{\Omega}$. Furthermore, assume that $\partial\Omega$ is of class C^{k-1} . Then there exists a scalar function $\mathcal{G}(\Gamma_\Omega) \subset \mathcal{D}^{-k}(\Gamma_\Omega)$ such that

$$(5.3) \quad D_{\Omega, \boldsymbol{\theta}} \mathcal{L}(\Omega) = \int_{\Gamma_\Omega} \mathcal{G} \boldsymbol{\theta} \cdot \mathbf{n} \, ds.$$

It therefore follows from the above lemma and (5.2) that

$$(5.4) \quad (\nabla \tilde{\boldsymbol{\beta}}, \nabla \boldsymbol{\theta})_\Omega + (\tilde{\boldsymbol{\beta}}, \boldsymbol{\theta})_\Omega = - \int_{\Gamma_\Omega} \mathcal{G} \boldsymbol{\theta} \cdot \mathbf{n} \, ds.$$

Equation (5.4) indicates that, in strong form, we need to solve the following interface problem for $\tilde{\boldsymbol{\beta}}$,

$$(5.5) \quad -\Delta \tilde{\boldsymbol{\beta}} + \tilde{\boldsymbol{\beta}} = 0 \quad \text{in } \hat{\Omega},$$

$$(5.6) \quad [D_n \tilde{\boldsymbol{\beta}}]|_{\Gamma_\Omega} = -\mathcal{G} \quad \text{on } \Gamma_\Omega,$$

$$(5.7) \quad \llbracket \tilde{\boldsymbol{\beta}} \rrbracket = 0 \quad \text{on } \Gamma_\Omega,$$

$$(5.8) \quad \tilde{\boldsymbol{\beta}} = 0 \quad \text{on } \partial\hat{\Omega}.$$

Given that Γ_Ω is smooth and $\mathcal{G} \in H^{1/2}(\Gamma_\Omega)$, we also have the following regularity estimate:

$$(5.9) \quad \|\tilde{\boldsymbol{\beta}}\|_{H^1(\hat{\Omega})} + \|\tilde{\boldsymbol{\beta}}\|_{H^2(\hat{\Omega} \setminus \Gamma_\Omega)} \lesssim \|\mathcal{G}\|_{H^{1/2}(\Gamma_\Omega)},$$

(see [21]) and hence $\tilde{\boldsymbol{\beta}} \in H^1(\hat{\Omega}) \cap H^2(\hat{\Omega} \setminus \Gamma_\Omega)$.

5.1. Approximation of the steepest descent velocity using CutFem. To obtain a numerical approximation for the steepest descent velocity, we also use the CutFEM for interface problem [27] on a single mesh. We first define the finite element spaces. Given a closed $d-1$ manifold $\Gamma \subset \hat{\Omega}$, define $\Omega_\Gamma^+ \subset \hat{\Omega}$ be the intersection of the domain enclosed by Γ and Γ_f and define $\Omega_\Gamma^- = \hat{\Omega} \setminus \Omega_\Gamma^+$. Also define the finite element space V_h^+ and V_h^- by

$$V_h^+ = \{v^+ \in H^1(\Omega^+) : v^+|_K \in P^1(K) \quad \forall K \cap \Omega^+ \neq \emptyset\},$$

and

$$V_h^- = \{v^- \in H^1(\Omega^-) : v^-|_K \in P^1(K) \quad \forall K \cap \Omega^- \neq \emptyset\}.$$

Note that both V_h^+ and V_h^- are defined on ‘‘cut’’ elements $K \in \mathcal{T}_h$ such that $K \cap \Gamma \neq \emptyset$. The finite element solution for $\boldsymbol{\beta}$ is then to find $\boldsymbol{\beta}_h \in V_h^+ \times V_h^-$ such that

$$(5.10) \quad b_0(\boldsymbol{\beta}_h, \mathbf{v}) + j(\boldsymbol{\beta}_h, \mathbf{v}) = l(\mathbf{v}) \quad \forall \mathbf{v} \in V_h^+ \times V_h^-$$

where

$$(5.11) \quad \begin{aligned} b_0(\boldsymbol{\beta}, \mathbf{v}) &= (\nabla \boldsymbol{\beta}^+, \nabla \mathbf{v}^+)_{\Omega^+} + (\nabla \boldsymbol{\beta}^-, \nabla \mathbf{v}^-)_{\Omega^-} - \langle \{D_n \boldsymbol{\beta}\}, [\mathbf{v}] \rangle_{\Gamma_\Omega} - \langle D_n \boldsymbol{\beta}, \mathbf{v} \rangle_{\Gamma_f} \\ &\quad - \langle \{D_n \mathbf{v}\}, [\boldsymbol{\beta}] \rangle_{\Gamma_\Omega} + \beta_1 h^{-1} \langle [\boldsymbol{\beta}], [\mathbf{v}] \rangle_{\Gamma_\Omega} - \langle D_n \mathbf{v}, \boldsymbol{\beta} \rangle_{\Gamma_f} + \beta_2 h^{-1} \langle \boldsymbol{\beta}, \mathbf{v} \rangle_{\Gamma_f} \end{aligned}$$

$$(5.12) \quad j(\boldsymbol{\beta}, \mathbf{v}) = \gamma h \left(\sum_{F \in \mathcal{E}_I^+} \int_F [[D_n \boldsymbol{\beta}^+]] [[D_n \mathbf{v}^+]] + \sum_{F \in \mathcal{E}_I^-} \int_F [[D_n \boldsymbol{\beta}^-]] [[D_n \mathbf{v}^-]] \right)$$

and

$$(5.13) \quad l(\mathbf{v}) = -D_{\Omega, \mathbf{v}} \mathcal{L}_h \quad \text{or} \quad l(\mathbf{v}) = -\tilde{D}_{\Omega, \mathbf{v}} \mathcal{L}_h.$$

Here $\mathcal{E}_I^\pm = \{F : F \in \mathcal{E}_I, K \cap \Omega_\Gamma^\pm \neq \emptyset, K' \cap \Omega_\Gamma^\pm \neq \emptyset \text{ where } K \cap K' = F\}$.

5.2. Level set update. With the steepest direction on hand, we now aim to update the free boundary. By introducing the pseudo-time, we aim to find the level set function $\phi(x + t\boldsymbol{\beta}(x), t)$ for some given $\boldsymbol{\beta}$ such that

$$\phi(x + t\boldsymbol{\beta}(x), t) = \phi(x, 0) \quad \forall t \text{ and } \forall x \in \hat{\Omega}.$$

Taking the derivative with respect to t gives that

$$\nabla_x \phi \cdot \boldsymbol{\beta} + \frac{\partial \phi}{\partial t} = 0,$$

which yields a Hamilton-Jacobi equation, if the nonlinear dependence of $\boldsymbol{\beta}$ on the optimization is accounted for. However for fixed vector field $\boldsymbol{\beta}$ this is simply an advection problem with a non-solenoidal transport field.

Remark 5.1. Note that the level set function chosen at the initial stage is the distance function. However, after evolution steps the updated level set function no longer holds the property of a distance function. This could cause potential problems, for accuracy if the magnitude of the gradient locally becomes very small and for the stability of the numerical scheme if the gradient becomes very large. It is well known that the issue can be resolved by redefining ϕ regularly as the distance function while keeping the interface position fixed. In the numerical examples presented herein we did not notice any need for re-distancing, since an advection stable scheme was used to propagate the interface.

To approximate the Hamilton-Jacobi equation, we use Crank-Nicolson scheme in time combining with gradient penalty stabilization in space for the advection problem [18, 14]. We keep the same background mesh for the transport of the level set function.

For each Ω , let $T = r * \frac{J(\Omega)}{\|\beta_h\|_{H^1(\hat{\Omega})}}$, where r is the learning rate. First divide $[0, T]$ into N equal length steps and let $\delta t = T/N$ and $t_i = i\delta t$ for $i = 0, \dots, N$. Denote by $\phi_h^n = \phi_h(t_n)$. Given the initial level set ϕ_h^0 , find $\phi_h^n \in V_h$ for $n = 1, \dots, N$ such that

$$(5.14) \quad \left(\frac{\phi_h^n - \phi_h^{n-1}}{\delta t}, w \right)_D + \left(\beta_h \cdot \nabla \frac{\phi_h^n + \phi_h^{n-1}}{2}, w \right)_D + r_h \left(\frac{\phi_h^n + \phi_h^{n-1}}{2}, w \right)$$

where

$$r_h(v, w) = \sum_{F \in \mathcal{E}_I} \gamma_2 h^2 \int_F [[D_n v]] [[D_n w]] ds$$

with $\gamma_2 > 0$ is a parameter and \mathcal{E}_I is the set of all interior facets in \mathcal{T}_0 . In the numerics, we chose $r = 1.0$ or 0.5 , $N = 10$ and $\gamma_2 = 1.0$.

Below we summarize the algorithm.

Algorithm 5.1 Bernoulli Free Boundary Identification

Input an initial level set ϕ_h and specify the tolerance.

while $J > \text{tolerance}$ **do**

 Compute the primal solution u_h by (3.4) and the dual solution p_h by (3.5).

 Compute J .

 Compute the velocity β_h by (5.10).

 Compute $T = r * \frac{J}{\|\beta_h\|_{H^1(\hat{\Omega})}}$. ($0 < r < 1$ is the learning rate).

 Normalize β_h .

 Compute $\phi_h(x, T)$ by (5.14).

 Set $\phi_h(x, 0) = \phi_h(x, T)$.

end while

6. Numerical experiments. In the numerical experiments we mainly aim to compare the performances of the three different shape derivatives, i.e., the classical shape derivative (SD) given in (4.20) obtained based on the first optimize then discretize approach, (4.28) obtained based on the first discretize then optimize approach, and the (4.41) obtained based on the boundary correction approach. For simplicity, in this section we refer the three shape derivatives as the *continuous SD*, *discrete SD* and *boundary SD*.

For the CutFEM method a regular fixed background mesh is used. For all numerical experiments in this paper we will use the unit square domain as the background

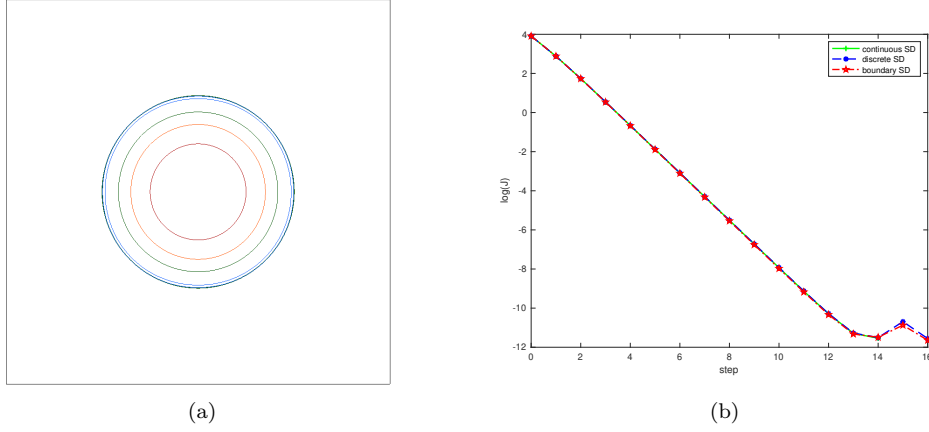


FIG. 2. *Example 6.1*: (a): level sets at steps 0, 1, 2, 5 and 10; (b): the comparison of residual evolution

domain, i.e., $\hat{\Omega} = [0, 1]^2$ and the background mesh is a uniform 100×100 mesh. The penalty parameters in (3.1) are chosen as $\gamma = 0.1$ and $\beta = 10$. And in (5.10), the parameters are chosen such that $\beta_1 = \beta_2 = 10.0$ and $\gamma = 1.0$.

Example 6.1 (Circle). We recall the problem:

$$(6.1) \quad \begin{aligned} -\Delta u &= f && \text{in } \Omega, \\ u &= 0 && \text{on } \Gamma_{\Omega}, \\ u &= g_D, \quad D_n u = g_N && \text{on } \Gamma_f. \end{aligned}$$

For this example, the free boundary Γ_{Ω} is the circle with radius $r = 1/4$ and center being $(0.5, 0.5)$.

We chose to use the following data set:

$$(6.2) \quad u = 4r - 1 \text{ and } f = -4/r.$$

We note that the data set is not unique and indeed there are infinitely many choices.

We start with the following initial level set:

$$\phi(r, \theta) = -r + 1/8,$$

which is a smaller circle with the same center as the true interface (see the inner most red circle in Figure 2a).

The stopping criteria is set such that $J(\Omega) \leq 1E-5$. It takes 14, 16 and 16 steps, respectively, using the continuous SD, discrete SD and boundary SD to reach the stopping criteria. In this case, the performances between those three shape derivatives are almost identical. Figure 2a shows the level sets at steps 0, 1, 2, 5 and 10 (from the inner most to the outer most circles) for all three shape derivatives. The level set at step 0 is the initial guess of level set. At step 10, the computed level set almost coincides with the true level set. Figure 2b shows the decreasing log rate of the residuals. In this case all residuals converge at a uniform rate.

We now test with an initial level set as an ellipse (see the red curve in Figure 3a):

$$\phi(x, y) = -\frac{(x-0.5)^2}{c_1^2} - \frac{(x-0.5)^2}{c_2^2} + 1, \text{ where } c_1 = 3/8, \text{ and } c_2 = 1/8.$$

Figure 3a - Figure 3e show the obtained level sets at steps 0, 5, 10, 20 and 50 using the continuous SD (green), discrete SD (blue) and boundary SD (red). With the same stopping criteria that $J \leq 1E - 5$, it takes 169, 155, and 123 steps respectively for the continuous SD, discrete SD and boundary SD. We note that in this case using the boundary SD shows slightly better performance.

In Figure 3f we compare the residual evolution for the first 100 steps. We note that there are two different convergence patterns for all shape derivatives: in the first 20 steps the residual is decreasing at a uniform fast rate and afterwards evolves at a much slower rate.

If the initial guess is not properly chosen, the iterative procedure might need much more steps to converge. Moreover, since we are using a gradient method, the minimum obtained is a local minimum. We also note that it is natural that the residual oscillates when the pseudo time step is fixed. Also observe that although the SD may be exact for the discrete formulation it is not necessarily in the finite element space and must nevertheless be approximated.

Example 6.2 (Ellipse). For this example, the free boundary Γ_Ω is an ellipse (see the magenta curve in Figure 4a) with the following level set representation:

$$\phi(x, y) = -16(x - 0.5)^2 - 64(y - 0.5)^2 + 1.$$

We chose to use the data set such that $f = 0$, $g_N = (\sin(x + y), \cos(x + y)) \cdot \mathbf{n}$ and g_D is obtained by solving the forward problem on a 500×500 mesh.

We start with an initial level set of a circle (see the red circle in Figure 4a):

$$\phi(x, y) = -\sqrt{(x - 0.6)^2 + (y - 0.4)^2} + 1/6,$$

which is partially intersected with the true interface. Figure 4a–Figure 4e show the obtained level sets at steps 0, 5, 10, 50 and 120 using the continuous SD (green), discrete SD (blue) and the boundary SD (red). With the stopping criteria that $J \leq 1E - 5$, it takes 120, 154, and 146 steps respectively for the continuous SD, discrete SD and boundary SD. We again observe that the level sets and the residual evolution of three methods are all very similar. However, the number of steps that it takes to reach the stopping criteria could differ quite a lot due to its slow convergence rate and oscillating character of the cost functional.

Example 6.3 (Lamé Square). For this example the free boundary Γ_Ω is a Lamé Square that has the following level set representation (see the magenta curve in Figure 5a):

$$\phi(x, y) = -81(x - 0.5)^n - 1296(y - 0.5)^n + 1, \quad n = 4.$$

The level set becomes closer to a rectangle as the integer n increases. We chose the data such that $f = 0$, $g_N = (5 \sin(\theta), 5 \cos(\theta)) \cdot \mathbf{n}$ where $\theta = \tan^{-1}((y - 0.5)/(x - 0.5))$ and g_D is obtained by solving the forward problem on a 500×500 mesh.

We firstly start with circle as the initial level set, (see the red circle in Figure 5a)

$$\phi(x, y) = -\sqrt{(x - 0.5)^2 + (y - 0.5)^2} + 1/8.$$

Figure 5b–Figure 5f show the level sets at steps 5, 10 and 50 and 150 obtained by the continuous SD (green), discrete SD (blue) and boundary SD (red). With the stopping criteria that $J \leq 5E - 6$ and maximal iteration number not exceeds 200, it takes 173, 174, and 200 steps respectively using the continuous SD, discrete SD and boundary SD. In this case, again, continuous and discrete SDs behaves almost identical. However, the level sets produced by the modified SD are slightly different.

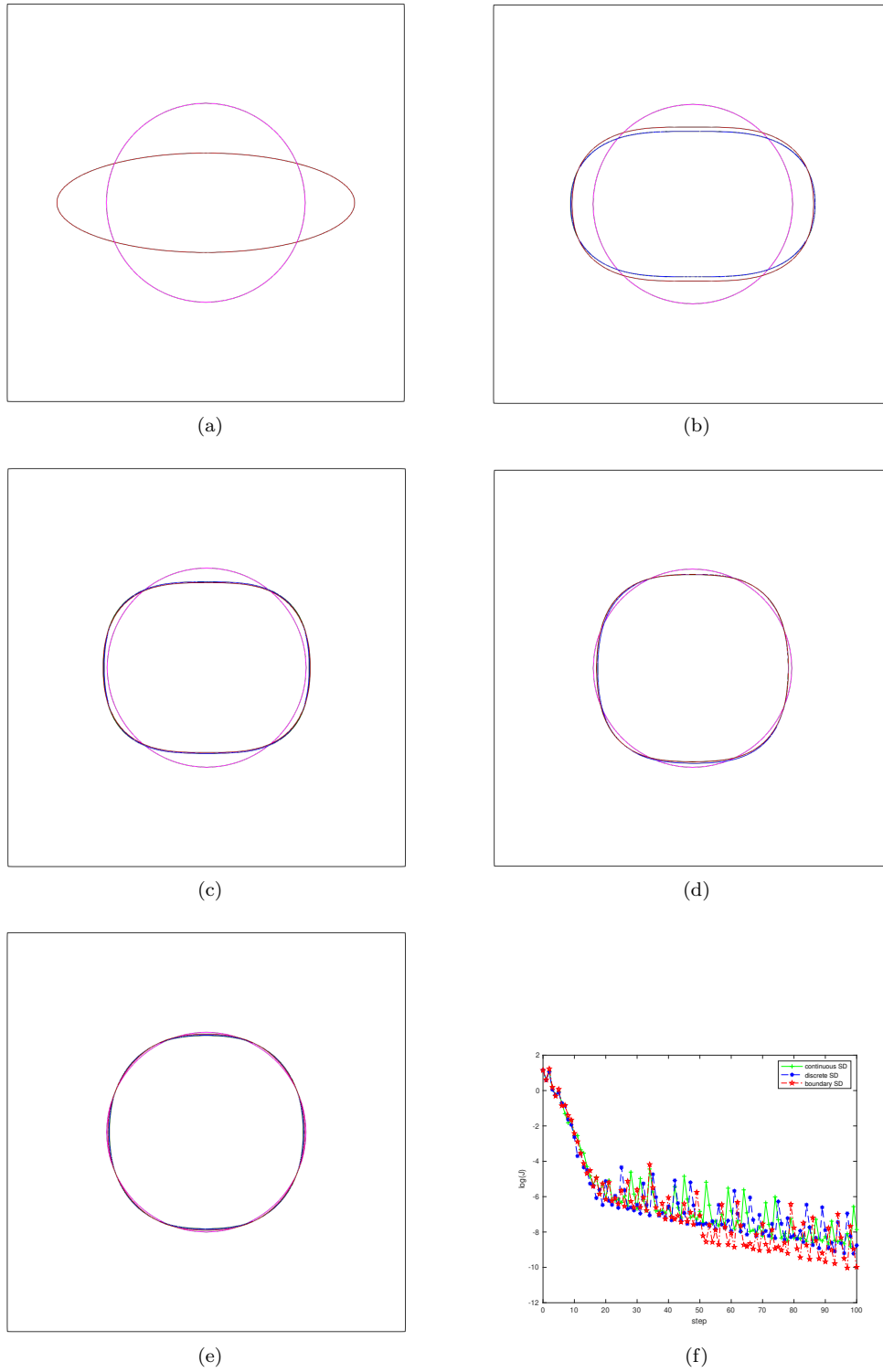


FIG. 3. *Example 6.1*: level sets at steps 0(a), 5(b), 10(c), 20(d), 50(e) and the comparison of residual evolution (d)

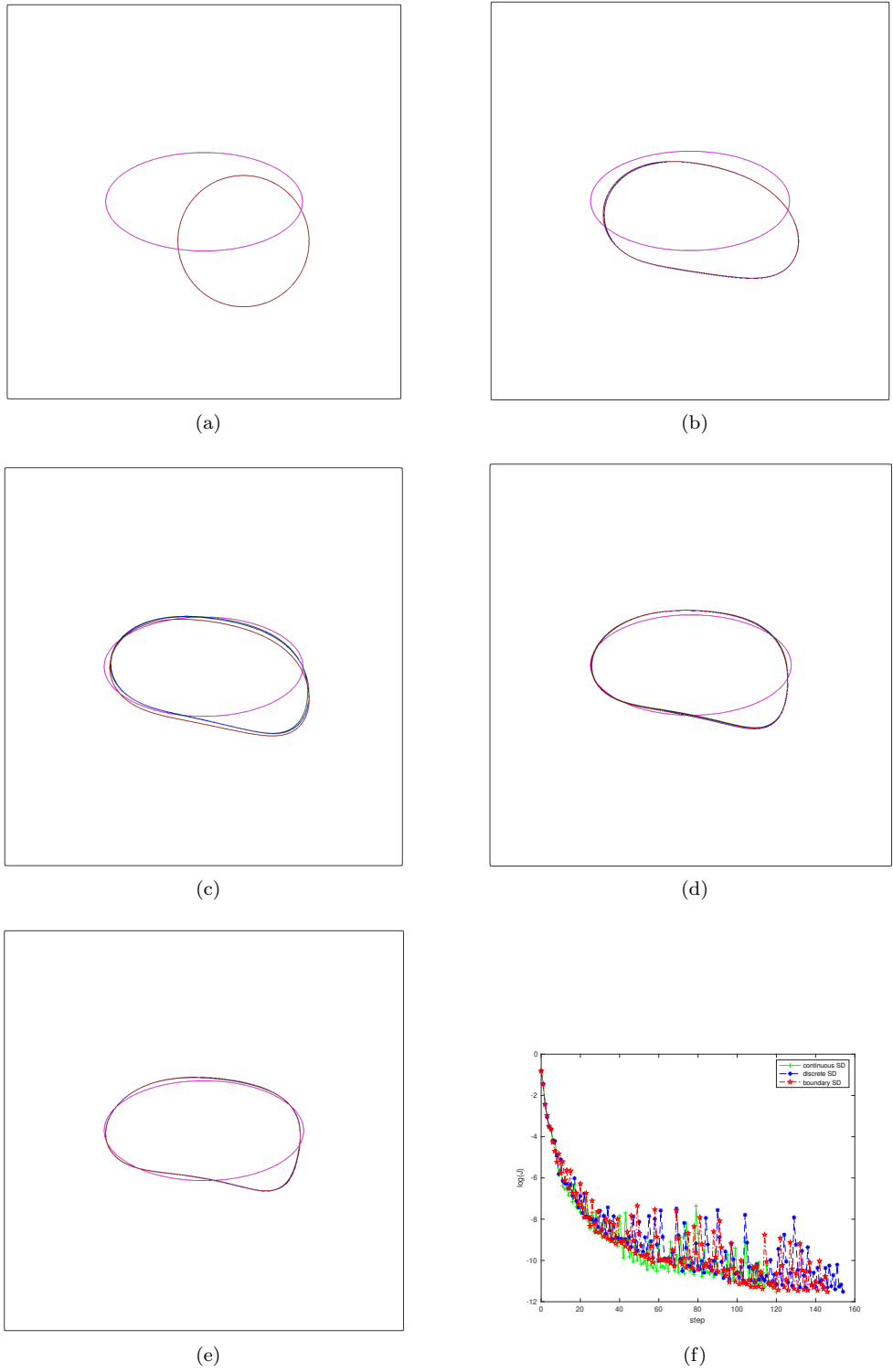


FIG. 4. *Example 6.2*: level sets at steps 0(a), 5(b), 10(c), 50(d) and 120(e) and the comparison of residual evolution (f)

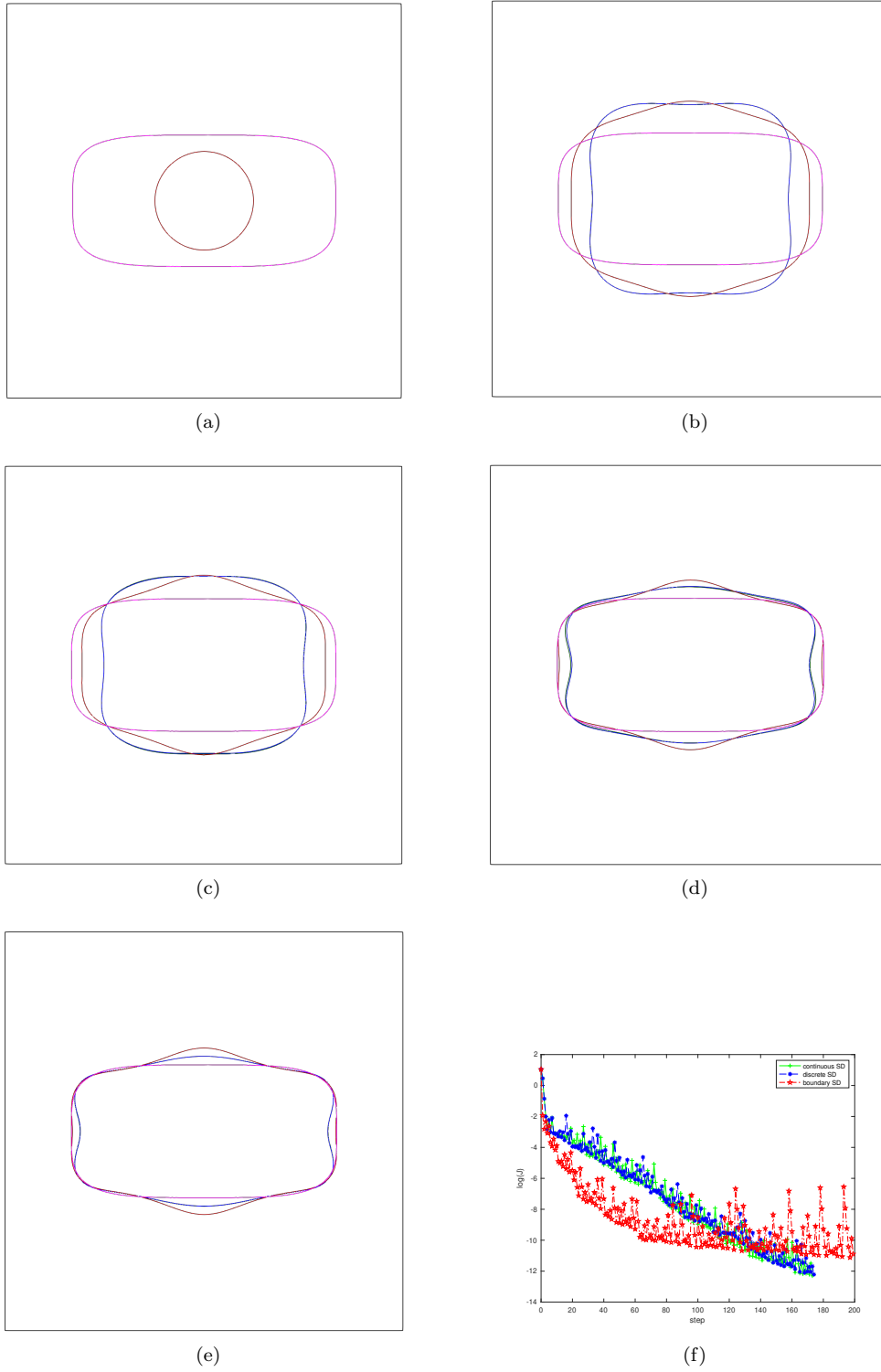


FIG. 5. *Example 6.3*: level sets at steps 0(a), 5(b), 10(c), 50(d) and 150(e) and the comparison of residual evolution (f)

Example 6.4 (Topology change of merging). In this test, we aim to validate the ability of topology change for our algorithm. We start with an initial guess of two separate Lamé squares with the following initial level set (see the red curves in [Figure 6a](#)):

$$\phi(x, y) = \max(\phi_1(x, y), \phi_2(x, y)),$$

where $\phi_1(x, y) = 1 - 1296(x - 0.32)^4 - 1296(y - 0.5)^4$ and $\phi_2(x, y) = 1 - 1296(x - 0.68)^4 - 1296(y - 0.5)^4$. The stopping criteria is set such that $J \leq 5E - 6$. It takes 271, 276, and 129 steps for the respective continuous SD, discrete SD and boundary SD to reach the stopping criteria. [Figure 6a](#) -[Figure 6e](#) show the level sets at the respective steps 0, 10, 50, 100 and the last step of level sets obtained by the continuous SD (green), discrete SD (blue) and boundary SD (red). We observe the topology change of merging in this case.

Example 6.5 (Doubly connected domain). In this example, we aim to identify the following level set with two isolated circles (see the magenta curve in [Figure 7a](#)):

$$\phi(x, y) = \max\left(0.15 - \sqrt{(x - 0.2)^2 + (y - 0.5)^2}, 0.15 - \sqrt{(x - 0.80)^2 + (y - 0.5)^2}\right).$$

We firstly test with a connected Cassini oval (see the red curve in [Figure 7a](#)):

$$\phi(x, y) = -(\hat{x}^2 + \hat{y}^2)^2 + 2(\hat{x}^2 - \hat{y}^2) - 1 + b^4, \quad \hat{x} = 3x - 1.5, \quad \hat{y} = 3y - 1.5, \quad b = 1.001.$$

The stopping criteria is set such that the maximal number of iteration not exceeds 300. We chose the data such that $f = 0$, $g_N = (x - 0.5, y - 0.5) \cdot \mathbf{n}$ and g_D is obtained by solving the forward problem on a 500×500 mesh. [Figures 7b-7d](#) show the level sets at the respective steps 50, 100, 200 and 300. This example validates the capability of the algorithm in the topology change of splitting. During the process, the Cassini oval initially splits into two cone-like shapes and then each gradually evolve into a circle. The convergence is, however, quite slow and it is likely due to the sharp angles evolved after splitting. The results generated by the three SDs are again quite similar.

7. Appendix. Proof of [Lemma 4.4](#)

Proof. By the assumption that T_t is smooth, using similar arguments as in [Lemma 4.1](#) and [Lemma 4.2](#) gives

$$\begin{aligned} & \int_{F^t} \llbracket \nabla w \cdot \mathbf{n}_t \rrbracket \llbracket \nabla v \cdot \mathbf{n}_t \rrbracket ds \\ (7.1) \quad &= \int_F \llbracket \nabla w \circ T^t \cdot (\mathbf{n}_t \circ T_t) \rrbracket \llbracket \nabla v \circ T^t \cdot (\mathbf{n}_t \circ T_t) \rrbracket \omega(t) ds \\ &= \int_F \llbracket A(t) \nabla(w \circ T^t) \cdot \mathbf{n} \rrbracket \llbracket A(t) \nabla(v \circ T^t) \cdot \mathbf{n} \rrbracket \omega^{-1}(t) ds \end{aligned}$$

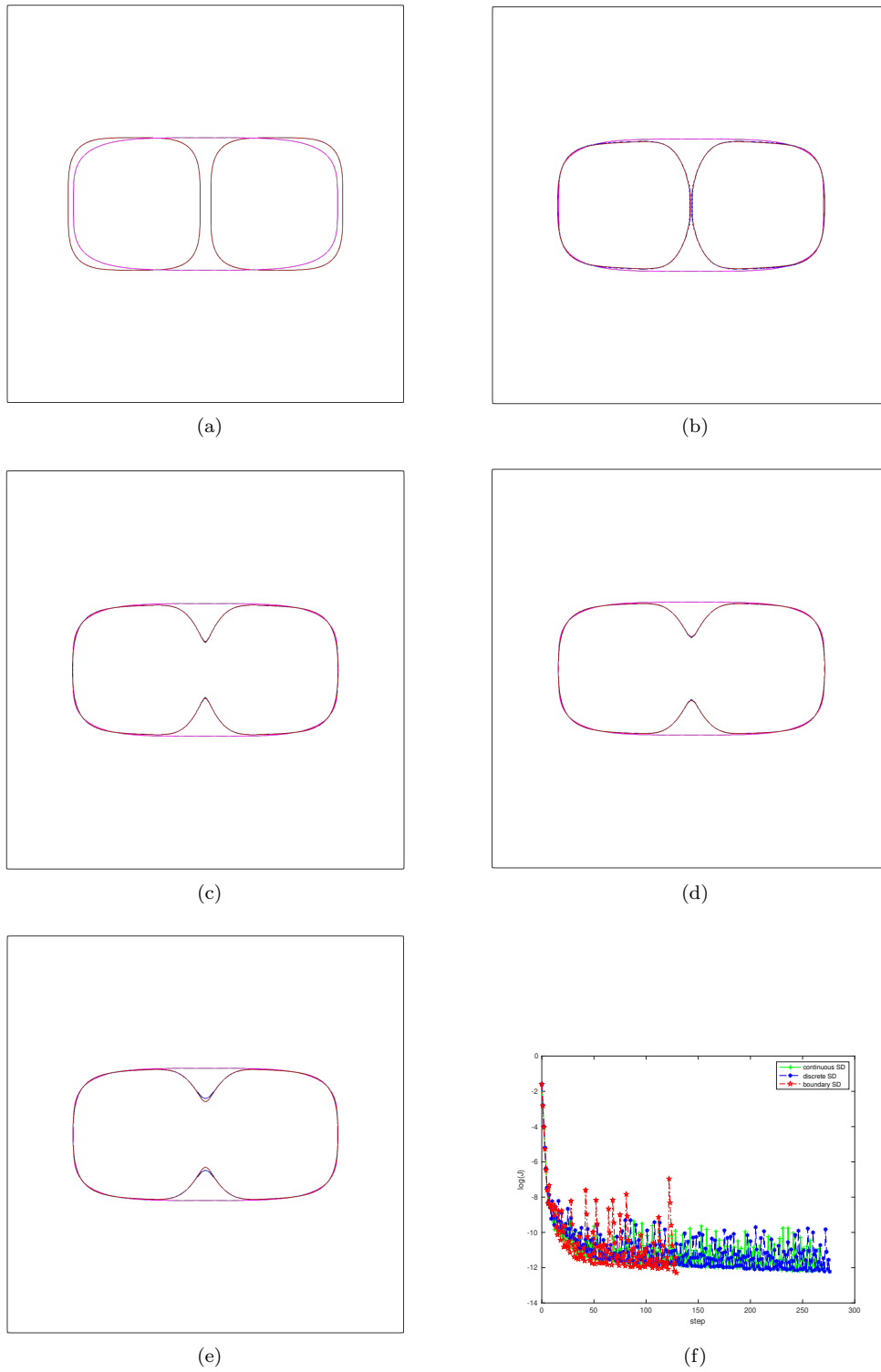
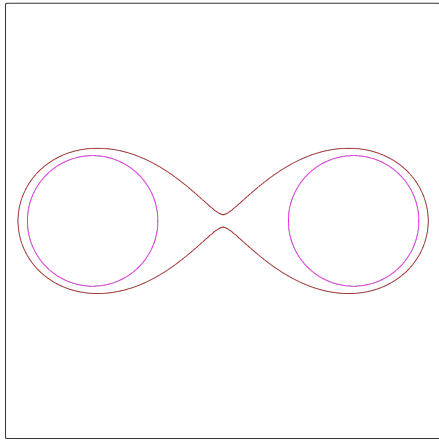
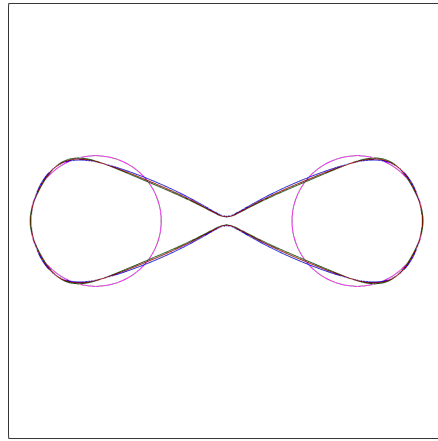


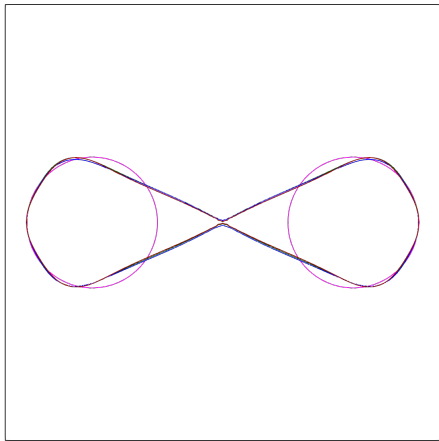
FIG. 6. *Example 6.3*: at steps 0(a), 10(b), 50(c), 100(d), the final (e), and the comparison of residual evolution (f) .



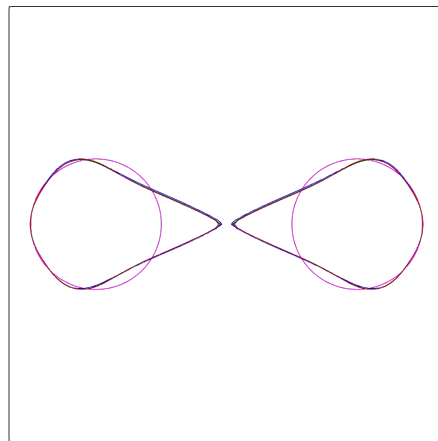
(a)



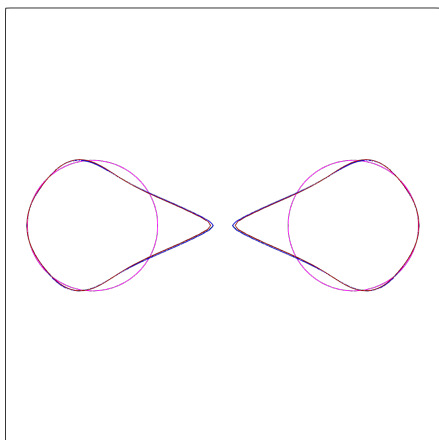
(b)



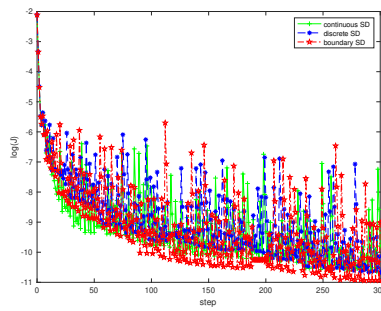
(c)



(d)



(e)



(f)

FIG. 7. *Example 6.5: at steps 0(a), 50(b), 100(c), 200(d) and 300(e) and the residual evolution*

Applying product rule, we then have that

$$\begin{aligned}
 & D_{\Omega, \theta} \int_F \llbracket \nabla w \cdot \mathbf{n} \rrbracket \llbracket \nabla v \cdot \mathbf{n} \rrbracket ds \\
 &= \int_F \llbracket A'(0) \nabla w \cdot \mathbf{n} \rrbracket \llbracket \nabla v \cdot \mathbf{n} \rrbracket + \llbracket A'(0) \nabla v \cdot \mathbf{n} \rrbracket \llbracket \nabla w \cdot \mathbf{n} \rrbracket \\
 &\quad + \int_F \llbracket \nabla w \cdot \mathbf{n} \rrbracket \llbracket \nabla \dot{v} \cdot \mathbf{n} \rrbracket + \llbracket \nabla v \cdot \mathbf{n} \rrbracket \llbracket \nabla \dot{w} \cdot \mathbf{n} \rrbracket ds \\
 (7.2) \quad & - \int_F \llbracket \nabla w \cdot \mathbf{n} \rrbracket \llbracket \nabla v \cdot \mathbf{n} \rrbracket \omega'(0) ds \\
 &= \int_F \llbracket (\nabla \cdot \theta) \nabla w \cdot \mathbf{n} - S(\theta) \cdot \nabla w \cdot \mathbf{n} \rrbracket \llbracket \nabla v \cdot \mathbf{n} \rrbracket ds + \int_F \llbracket \nabla \dot{w} \cdot \mathbf{n} \rrbracket \llbracket \nabla v \cdot \mathbf{n} \rrbracket ds \\
 &\quad + \int_F \llbracket (\nabla \cdot \theta) \nabla v \cdot \mathbf{n} - S(\theta) \cdot \nabla v \cdot \mathbf{n} \rrbracket \llbracket \nabla w \cdot \mathbf{n} \rrbracket ds + \int_F \llbracket \nabla w \cdot \mathbf{n} \rrbracket \llbracket \nabla \dot{v} \cdot \mathbf{n} \rrbracket ds \\
 &\quad - \int_F \llbracket \nabla w \cdot \mathbf{n} \rrbracket \llbracket \nabla v \cdot \mathbf{n} \rrbracket (\nabla \cdot \theta - (D\theta \cdot \mathbf{n}) \cdot \mathbf{n}) ds.
 \end{aligned}$$

This completes the proof of [Lemma 4.3](#). \square

REFERENCES

- [1] L. AFRAITES, M. DAMBRINE, K. EPPLER, AND D. KATEB, *Detecting perfectly insulated obstacles by shape optimization techniques of order two*, DISCRETE AND CONTINUOUS DYNAMICAL SYSTEMS SERIES B, 8 (2007), p. 389.
- [2] G. ALLAIRE, F. JOUVE, AND A.-M. TOADER, *A level-set method for shape optimization*, C. R. Math. Acad. Sci. Paris, 334 (2002), pp. 1125–1130, [https://doi.org/10.1016/S1631-073X\(02\)02412-3](https://doi.org/10.1016/S1631-073X(02)02412-3), [https://doi.org/10.1016/S1631-073X\(02\)02412-3](https://doi.org/10.1016/S1631-073X(02)02412-3).
- [3] G. ALLAIRE, F. JOUVE, AND A.-M. TOADER, *Structural optimization using sensitivity analysis and a level-set method*, J. Comput. Phys., 194 (2004), pp. 363–393, <https://doi.org/10.1016/j.jcp.2003.09.032>, <https://doi.org/10.1016/j.jcp.2003.09.032>.
- [4] A. BERNLAND, E. WADBRO, AND M. BERGGREN, *Acoustic shape optimization using cut finite elements*, International Journal for Numerical Methods in Engineering, 113 (2018), pp. 432–449.
- [5] F. BOUCHON, S. CLAIN, AND R. TOUZANI, *Numerical solution of the free boundary Bernoulli problem using a level set formulation*, Comput. Methods Appl. Mech. Engrg., 194 (2005), pp. 3934–3948, <https://doi.org/10.1016/j.cma.2004.09.008>, <https://doi.org/10.1016/j.cma.2004.09.008>.
- [6] F. BOUCHON, S. CLAIN, AND R. TOUZANI, *A perturbation method for the numerical solution of the Bernoulli problem*, J. Comput. Math., 26 (2008), pp. 23–36.
- [7] L. BOURGEOIS AND J. DARDÉ, *A quasi-reversibility approach to solve the inverse obstacle problem*, Inverse Probl. Imaging, 4 (2010), pp. 351–377, <https://doi.org/10.3934/ipi.2010.4.351>, <https://doi.org/10.3934/ipi.2010.4.351>.
- [8] L. BOURGEOIS AND J. DARDÉ, *The “exterior approach” to solve the inverse obstacle problem for the Stokes system*, Inverse Probl. Imaging, 8 (2014), pp. 23–51, <https://doi.org/10.3934/ipi.2014.8.23>, <https://doi.org/10.3934/ipi.2014.8.23>.
- [9] J. H. BRAMBLE, T. DUPONT, AND V. THOMÉE, *Projection methods for Dirichlet’s problem in approximating polygonal domains with boundary-value corrections*, Math. Comp., 26 (1972), pp. 869–879, <https://doi.org/10.2307/2005869>, <https://doi.org/10.2307/2005869>.
- [10] M. BURGER, *A level set method for inverse problems*, Inverse Problems, 17 (2001), pp. 1327–1355, <https://doi.org/10.1088/0266-5611/17/5/307>, <https://doi.org/10.1088/0266-5611/17/5/307>.
- [11] M. BURGER, *Levenberg-Marquardt level set methods for inverse obstacle problems*, Inverse Problems, 20 (2004), pp. 259–282, <https://doi.org/10.1088/0266-5611/20/1/016>, <https://doi.org/10.1088/0266-5611/20/1/016>.
- [12] M. BURGER AND S. J. OSHER, *A survey on level set methods for inverse problems and optimal design*, European journal of applied mathematics, 16 (2005), pp. 263–301.
- [13] E. BURMAN, *Ghost penalty*, Comptes Rendus Mathématique, 348 (2010), pp. 1217–1220.

- [14] E. BURMAN, *Crank-Nicolson finite element methods using symmetric stabilization with an application to optimal control problems subject to transient advection-diffusion equations*, *Commun. Math. Sci.*, 9 (2011), pp. 319–329, <http://projecteuclid.org/euclid.cms/1294170338>.
- [15] E. BURMAN, D. ELFVÉRSÓN, P. HANSBO, M. G. LARSON, AND K. LARSSON, *A cut finite element method for the Bernoulli free boundary value problem*, *Comput. Methods Appl. Mech. Engrg.*, 317 (2017), pp. 598–618, <https://doi.org/10.1016/j.cma.2016.12.021>, <https://doi.org/10.1016/j.cma.2016.12.021>.
- [16] E. BURMAN, D. ELFVÉRSÓN, P. HANSBO, M. G. LARSON, AND K. LARSSON, *Shape optimization using the cut finite element method*, *Computer Methods in Applied Mechanics and Engineering*, 328 (2018), pp. 242–261.
- [17] E. BURMAN, D. ELFVÉRSÓN, P. HANSBO, M. G. LARSON, AND K. LARSSON, *Cut topology optimization for linear elasticity with coupling to parametric nondesign domain regions*, *Comput. Methods Appl. Mech. Engrg.*, 350 (2019), pp. 462–479, <https://doi.org/10.1016/j.cma.2019.03.016>, <https://doi.org/10.1016/j.cma.2019.03.016>.
- [18] E. BURMAN AND M. A. FERNÁNDEZ, *Finite element methods with symmetric stabilization for the transient convection-diffusion-reaction equation*, *Comput. Methods Appl. Mech. Engrg.*, 198 (2009), pp. 2508–2519, <https://doi.org/10.1016/j.cma.2009.02.011>, <https://doi.org/10.1016/j.cma.2009.02.011>.
- [19] E. BURMAN, P. HANSBO, AND M. G. LARSON, *A cut finite element method with boundary value correction*, *Math. Comp.*, 87 (2018), pp. 633–657, <https://doi.org/10.1090/mcom/3240>, <https://doi.org/10.1090/mcom/3240>.
- [20] E. BURMAN, P. HANSBO, AND M. G. LARSON, *Dirichlet boundary value correction using lagrange multipliers*, *BIT Numerical Mathematics*, (2019), <https://doi.org/10.1007/s10543-019-00773-4>, <https://doi.org/10.1007/s10543-019-00773-4>.
- [21] Z. CHEN AND J. ZOU, *Finite element methods and their convergence for elliptic and parabolic interface problems*, *Numer. Math.*, 79 (1998), pp. 175–202, <https://doi.org/10.1007/s002110050336>, <https://doi.org/10.1007/s002110050336>.
- [22] J. CHEUNG, M. PEREGO, P. BOCHEV, AND M. GUNZBURGER, *Optimally accurate higher-order finite element methods for polytopial approximations of domains with smooth boundaries*, *Mathematics of Computation*, 88 (2019), pp. 2187–2219.
- [23] D. COLTON AND R. KRESS, *Looking back on inverse scattering theory*, *SIAM Rev.*, 60 (2018), pp. 779–807, <https://doi.org/10.1137/17M1144763>, <https://doi.org/10.1137/17M1144763>.
- [24] M. C. DELFOUR AND J.-P. ZOLÉSIO, *Shapes and geometries*, vol. 22 of *Advances in Design and Control*, Society for Industrial and Applied Mathematics (SIAM), Philadelphia, PA, second ed., 2011, <https://doi.org/10.1137/1.9780898719826>, <https://doi.org/10.1137/1.9780898719826>. Metrics, analysis, differential calculus, and optimization.
- [25] T. DUPONT, J. GUZMAN, AND R. SCOTT, *Obtaining higher-order Galerkin accuracy when the boundary is polygonally approximated*, *arXiv e-prints*, (2020), arXiv:2001.03082, p. arXiv:2001.03082, <https://arxiv.org/abs/2001.03082>.
- [26] J. HADAMARD, *Mémoire sur le problème d'analyse relatif à l'équilibre des plaques élastiques encastrées*, vol. 33, Imprimerie nationale, 1908.
- [27] A. HANSBO AND P. HANSBO, *An unfitted finite element method, based on Nitsche's method, for elliptic interface problems*, *Comput. Methods Appl. Mech. Engrg.*, 191 (2002), pp. 5537–5552, [https://doi.org/10.1016/S0045-7825\(02\)00524-8](https://doi.org/10.1016/S0045-7825(02)00524-8), [https://doi.org/10.1016/S0045-7825\(02\)00524-8](https://doi.org/10.1016/S0045-7825(02)00524-8).
- [28] R. HIPTMAIR AND A. PAGANINI, *Shape optimization by pursuing diffeomorphisms*, *Computational Methods in Applied Mathematics*, 15 (2015), pp. 291–305.
- [29] R. HIPTMAIR, A. PAGANINI, AND S. SARGHEINI, *Comparison of approximate shape gradients*, *BIT Numerical Mathematics*, 55 (2015), pp. 459–485.
- [30] A. LAURAIN AND K. STURM, *Distributed shape derivative via averaged adjoint method and applications*, *ESAIM: Mathematical Modelling and Numerical Analysis*, 50 (2016), pp. 1241–1267.
- [31] A. MAIN AND G. SCOVAZZI, *The shifted boundary method for embedded domain computations. part i: Poisson and stokes problems*, *Journal of Computational Physics*, 372 (2018), pp. 972–995.
- [32] J. NITSCHÉ, *Über ein variationsprinzip zur lösung von dirichlet-problemen bei verwendung von teilräumen, die keinen randbedingungen unterworfen sind*, in *Abhandlungen aus dem mathematischen Seminar der Universität Hamburg*, vol. 36, Springer, 1971, pp. 9–15.
- [33] S. OSHER AND R. P. FEDKIW, *Level set methods: an overview and some recent results*, *Journal of Computational physics*, 169 (2001), pp. 463–502.
- [34] D. PENG, B. MERRIMAN, S. OSHER, H. ZHAO, AND M. KANG, *A pde-based fast local level set*

- method*, Journal of computational physics, 155 (1999), pp. 410–438.
- [35] J. SOKOLOWSKI AND J.-P. ZOLÉSIO, *Introduction to shape optimization*, vol. 16 of Springer Series in Computational Mathematics, Springer-Verlag, Berlin, 1992, <https://doi.org/10.1007/978-3-642-58106-9>, <https://doi.org/10.1007/978-3-642-58106-9>. Shape sensitivity analysis.
- [36] C. H. VILLANUEVA AND K. MAUTE, *CutFEM topology optimization of 3D laminar incompressible flow problems*, Comput. Methods Appl. Mech. Engrg., 320 (2017), pp. 444–473, <https://doi.org/10.1016/j.cma.2017.03.007>, <https://doi.org/10.1016/j.cma.2017.03.007>.
- [37] M. Y. WANG, X. WANG, AND D. GUO, *A level set method for structural topology optimization*, Computer methods in applied mechanics and engineering, 192 (2003), pp. 227–246.